



# Formulation and Pathohistological Study of Mizolastine–Solid Lipid Nanoparticles–Loaded Ocular Hydrogels

Ghada Ahmed El-Emam <sup>1</sup>  
 Germeen NS Girgis <sup>1</sup>  
 Mohammed Fawzy Hamed <sup>2</sup>  
 Osama Abd El-Azeem Soliman<sup>1</sup>  
 Abd El Gawad H Abd El Gawad<sup>1</sup>

<sup>1</sup>Department of Pharmaceutics, Faculty of Pharmacy, Mansoura University, Mansoura, 35516, Egypt; <sup>2</sup>Department of Pathology, Faculty of Veterinary Medicine, Mansoura University, Mansoura, Egypt

**Background:** Mizolastine (MZL) is a dual-action nonsedating topical antihistamine anti-inflammatory agent that is used to relieve allergic conditions, such as rhinitis and conjunctivitis. Solid lipid nanoparticles (SLNs) are advanced delivery system in ophthalmology, with the merits of increasing the corneal drug absorption and hence improved bioavailability with the objective of ocular drug targeting.

**Methods:** First, MZL was formulated as MZL-SLNs by hot homogenization/ultrasonication adopting a 3<sup>2</sup> full factorial design. Solid-state characterization, in vitro release, and stability studies have been performed. Then, the optimized MZL-SLNs formula has been incorporated into ocular hydrogels using 1.5% w/v Na alginate and 5% w/v polyvinylpyrrolidone K<sub>90</sub>. The gels were evaluated via in vitro release as well as in vivo studies by applying allergic conjunctivitis congestion in a rabbit-eye model.

**Results:** The optimized formula (F4) was characterized by the highest entrapment efficiency (86.5±1.47%), the smallest mean particle size (202.3±13.59 nm), and reasonable zeta potential (−22.03±3.65 mV). Solid-state characterization of the encapsulation of MZL in SLNs was undertaken. In vitro results showed a sustained release profile from MZL-SLNs up to 30 hours with a non-Fickian Higuchi kinetic model. Stability studies confirmed immutability of freeze-dried MZL-SLNs (F4) upon storage for 6 months. Finally, hydrogel formulations containing MZL-SLNs, proved ocular congestion disappearance with completely repaired conjunctiva after 24 hours. Moreover, pretreatment with MZL-SLNs–loaded hydrogel imparted markedly decreased TNF-α and VEGF-expression levels in rabbits conjunctivae compared with post-treatment with the same formula.

**Conclusion:** MZL-SLNs could be considered a promising stable sustained-release nanoparticulate system for preparing ocular hydrogel as effective antiallergy ocular delivery systems.

**Keywords:** mizolastine, solid lipid nanoparticles, 3<sup>2</sup> full factorial design, sustained release, in vivo study

## Introduction

Currently existing topical antiallergy drugs are members of numerous pharmacological classes, such as: antihistamines, nonsteroidal anti-inflammatory agents, mast-cell stabilizers, dual-acting agents (mast-cell stabilizers with antihistamine action), vasoconstrictors, corticosteroids, and calcineurin inhibitors.

Mizolastine (MZL) is a new benzimidazole-derivative nonsedating antihistamine with additional antiinflammatory properties, that is used to relieve seasonal

Correspondence: Ghada Ahmed El-Emam  
 Department of Pharmaceutics, Faculty of Pharmacy, Mansoura University,  
 Mansoura, 35516, Egypt  
 Tel +20 10-9059-0989  
 Email ghadaelemam26@yahoo.com

and perennial allergic rhinitis. It is a peripherally acting, selective H<sub>1</sub>-receptor antagonist, recruitment neutrophil, vascular endothelial growth factor (VEGF), tissue necrosis factor (TNF- $\alpha$ ), 5-lipoxygenase.<sup>5,18</sup> It constrains the action of released histamine from activated mast cells, the chemotaxis of inflammatory cells, and the expression of intercellular adhesion molecule-1 (ICAM1) during an allergic reaction.<sup>61</sup> MZL is rapidly absorbed from the gastrointestinal tract, with peak plasma concentration of 0.3 mg/L being reached after about 1.5 hours. Plasma protein binding is about 98%. The mean elimination half-life is about 13 hours. It is water-insoluble (0.01 mg/mL), soluble in DMSO, and slightly soluble in methanol and chloroform by heating. It has pKa values of 9.99, 5.99, and 3.2 and it is classified according to the Biopharmaceutics Drug Disposition Classification System BDDCS as Class II (low solubility, high permeability). Yet, there is not any topical dosage form in the market containing MZL, and the only available form is (Lastlarge) tablets, 10 mg once daily.

MZL is among the dual-action topical antihistamines, which are nowadays the main effective therapy against the benign forms of allergic conjunctivitis. These agents have the advantage of providing rapid relief of symptoms by combining histamine receptor-antagonist action coupled with the long-term benefit of mast-cell stabilization (multimodal agents). These combined pathways offer both immediate and sustained relief during both early- and late-phase ocular allergic reactions.<sup>1</sup> A study performed by Bansal et al<sup>5</sup> revealed that controlled-release ocular inserts of MZL using Eudragit RL100 and RS100 which were capable of releasing the drug continuously at a controlled rate for 5 days.

Solid lipid nanoparticles (SLNs) are flexible nanocarriers used for drug delivery in almost all routes of administration, including; ocular, parenteral, oral, and dermal. They have ability to sustain the drug delivery profile and consequently decrease the frequency of administrations and improve the therapeutic effectiveness. In addition, they can improve drug bioavailability and achieve targeting.<sup>32</sup>

SLNs signify a motivating approach for ophthalmic drug delivery, as they can increase the corneal absorption of drugs, thus improving their bioavailability.<sup>43</sup> Moreover, their biocompatibility and mucoadhesiveness characters attain an improved ocular mucosa contact, with a prolonged drug corneal residence and objective ocular drug targeting.<sup>23</sup>

Allergic conjunctivitis is an inflammatory disease that influences the ocular surface: the lid, conjunctiva, and cornea. It is triggered by abnormal immunohypersensitivity reactions to environmental allergens. The immunomechanism of allergic conjunctivitis is characterized by IgE-mediated mast cell degranulation and/or T lymphocyte-mediated immunohypersensitivity response.<sup>12,34,58</sup>

The aim of this work was to formulate and evaluate MZL in SLNs using different lipid amounts and surfactant percentages. Furthermore, adopting a 3<sup>2</sup> randomized full factorial design to investigate the main influences and interactions of independent variables on the physicochemical properties of the prepared MZL-SLNs, ie, mean particle size (MPS), entrapment efficiency % (EE %), polydispersity index (PDI), and zeta potential (ZP). In addition, solid state characterization, in vitro release characteristics, and kinetics of the optimized formula, and the stability study at room and refrigerated temperatures for the lyophilized powder of the improved formula were investigated. Finally, the effects of the optimized MZL SLNs-based ophthalmic hydrogels on noninfectious allergic conjunctivitis in a rabbit model were applied.

## Materials and Methods

### Materials

MZL was provided by Medizen Pharmaceutical Industries, Borg El Arab city, Alexandria, Egypt. Glyceryl monostearate (GMS) pellets (melting point 57°–65°C), compritol ATO 888 (glyceryl behenate) (melting point 65°–77°C) and precirol ATO 5 (glyceryl palmitostearate) (melting point 50°–60°C) were obtained as a gift from Gattefoscé Co., Saint-Priest, Cedex, France. D-trehalose dihydrate was purchased from Sisco Research Pvt, LTD, Mumbai, India. Histamine acid phosphate was obtained from Universal Fine Chemicals, India. Sodium chloride, Tween 80 (polysorbate 80), propylene glycol, and stearic acid were kindly supplied by Adwic Pharmaceutical Chemicals, El Nasr, Egypt. Sodium lauryl sulfate (SLS) was supplied by Merck, Germany, and 3,3-diaminobenzidine tetrahydrochloride (DAB) was purchased from Dako, Glostrup, Denmark. Methanol of HPLC grade was purchased from Fisher Scientific, Germany. Sodium alginate was purchased from BDH Chemical, Liverpool, England). Methyl paraben and propyl paraben were obtained from Clariant Chemicals, Switzerland. Polyvinylpyrrolidone (PVP K<sub>90</sub>) was obtained from Sigma-Aldrich (Saint Louis, MO, USA).

### Lipid Selection for SLNs (Lipid–Water Partitioning)

Partitioning of drug between lipids and the aqueous phase was performed at a temperature above the melting point of each selected lipid, ie, precirol ATO 5, glyceryl monostearate (GMS), compritol ATO 888, and stearic acid. The mixture of lipid and water in the ratio of 1:1 (w/w) was stirred for one day to allow complete saturation, followed by the drug addition. Then, the mixture was stirred for 3 days at each specified temperature ( $75^{\circ}\pm 3^{\circ}\text{C}$ ). After cooling the mixture, the aqueous phase was separated, centrifuged (high-speed tabletop centrifuge model H1650-W, Ray Wild, Germany) at 6,000 rpm for 30 minutes and filtered. Spectrophotometric determination using an ultraviolet-visible spectrophotometer (model UV-1601 PC, Shimadzu, Kyoto, Japan) of the drug concentration in the aqueous phase and lipids was made.<sup>33</sup> The lipid possessed a high drug partitioning has been selected. The partition coefficient was calculated by using the Nernst equation

$$\text{P.C.} = \frac{C_o}{C_{aq}} \quad (1)$$

where; P.C, is the partition coefficient and  $C_o$  and  $C_{aq}$ : drug concentration in the lipid and aqueous phases, respectively.

### Preparation of MZL-SLNs

Hot homogenization method was used for SLNs preparation.<sup>24,37,38,60</sup> Temperature was adjusted to approximately  $5^{\circ}\text{C}$  above the melting point of GMS lipid at  $70^{\circ}\text{C}$  to ensure complete melting of the lipid. Then, MZL (10 mg) was dissolved in 2 mL methanol and added to the lipid melt at the same temperature. Aqueous sodium chloride (NaCl) solution 20 mL (0.1 M) containing Tween 80 (surfactant) having the same temperature was added, forming a hot pre-emulsion by high-speed stirring over a magnetic stirrer (Heidolph, USA, Table 1). The hot preemulsion was then processed in a controlled-temperature ultrasonic homogenizer (model VC505, Sonics & Materials, Inc., Newtown, CT, USA) and adjusted at its maximum amplitude (100%) for 5 minutes (one pulse on and one pulse off).

The acquired nanoemulsion was recrystallized upon cooling down to room temperature for 2 hours by continuous stirring for evaporation of the organic solvent. SLNs were collected by cooling centrifugation (CE16-4X100RD, Acculab, USA) at 13,000 rpm for 90 minutes and washed once with deionized water. All batches of SLNs were produced at least in triplicate.

For lyophilization of MZL-SLNs, the collected nanoparticles were resuspended in deionized water containing 5% (w/v) D-trehalose dehydrate. After this, they were prefrozen in a deep freezer at  $-8^{\circ}\text{C}$  overnight, then they were transferred to the lyophilizer (Labconco Lyph-Lock 4.5, USA) for 48 hours. Plain nanoparticles were prepared using identical procedure variables to be used as blanks. All samples were prepared in triplicate.

### Design of Experiment and Statistical Analysis

The design of experiment (DOE) approach was used to offer an efficient mean to optimize the hot homogenization process and discover the cause and the effect relationships between the processes variables and their outcomes in order to explore a mathematical correlation between factors and parameters.

Preliminary optimization was carried out to study the influence of process parameters, such as sonication time, concentration of lipids, and concentration of surfactant. Thereafter, plain SLNs and MZL-SLNs were prepared following a  $3^2$  randomized full factorial design to investigate the main influences and interactions of independent variables on the physicochemical properties of the prepared MZL-SLNs. Accordingly, nine possible combinations of experimental trials, each with three runs, were prepared.

Screening of MZL-SLNs dispersions using a three-level and two-variable with  $3^2$  full factorial design was the appropriate conditions for SLNs preparations.

For this design, lipid concentration A with three levels (300 mg, 400 mg, and 600 mg) and emulsifier concentration B with three levels (0.25%, 0.5%, and 1% w/w) were

**Table 1** Independent formulation variables and their levels applied using Design Expert

Factor	Name	Type	Low actual level	Medium actual level	High actual level	Low coded level	Medium coded level	High coded level
A	Lipid concentration	Numeric	300 mg	400 mg	600 mg	-1	0	+1
B	Surfactant concentration	Numeric	0.25%	0.5%	1%	-1	0	+1

selected as two critical process parameters (CPPs) [independent variables], (Table 1). Four responses were chosen to study their effect on particle size (PS), particle distribution, EE %, and ZP.

To understand the outcomes depending upon the values of magnitude of coefficients and the supplementary positive (synergistic effect) or negative sign (antagonistic effect),<sup>41</sup> a complete polynomial regression equation was conducted as follow:

$$Y = b_0 + b_1 A + b_2 B + b_3 AB + b_4 A^2 + b_5 B^2 \quad (2)$$

where;  $b_0$  is the intercept corresponding to the arithmetic average of quantitative outcomes of nine runs,  $b_1$  to  $b_5$  indicate coefficients calculated from the experimentally detected values of Y. Besides, A, and B corresponding to the coded levels of the independent variables. The term "AB" represents an interaction term that indicates modifications in the response parameters when two factors are concurrently changed. The main effects, A and B, symbolize the mean result when changing one factor at a time from its low to high value. Non-linearity in the model was furthermore examined by the polynomial terms  $A^2$  and  $B^2$ .

The model was assessed in expressions of statistical significance using ANOVA (Design Expert 12 (Stat-Ease, Minneapolis, MN, USA). Surface-response plots and contour plots were analyzed by preserving each factor at its low, medium, and high levels and varying the other factors over the range used in the study.

## Characterization of MZL-SLNs

All the nine MZL-SLNs formulae were subjected to assessment of PS, PDI, EE, and ZP. the results of critical quality attributes (CQAs) for various formulations have been recorded. The effect of CPPs on EE%, PS, and PDI were quantified through polynomial coded equations.

## MPS and PDI

PS and PDI values of all freshly prepared batches were measured by photon correlation spectroscopy (PCS) employing a Malvern Zetasizer (Zetasizer, Nano-ZS 90, Malvern, UK) after 1:10 dilution with deionized water to yield a suitable scattering intensity. Each measurement was repeated three times.

## Zeta Potential

Laser Doppler electrophoresis was used to evaluate particle electrophoretic movement through indirect determination of diffusion-layer thickness using the Nano-ZS 90.

Each sample was measured in triplicate after dilution at 25°C with the water refractive index fixed at 1.33.<sup>29</sup>

## Entrapment Efficiency

A weight of 100 mg of each lyophilized MZL-SLNs formulation was solubilized in 50 mL methanol in 50 mL volumetric flasks and sonicated for 15 minutes to liberate the drug, heated to 80°C, then suitably diluted with methanol.

The samples were filtered. The EE of MZL-SLNs was estimated using the spectrophotometer ( $\lambda_{\text{max}}=230$  nm). For each formulation, the results are presented as mean values of triplicate samplings. EE % was determined using the following equation:

$$\text{EE \%} = \frac{\text{Amount of entrapped MZL}}{\text{Total amount of MZL}} \times 100 \quad (3)$$

## Evaluation of Optimized (F4) of MZL-SLNs

### Transmission Electron Microscopy (TEM)

Morphological examination of suspended F4-SLNs was performed using TEM (JEM-2000EX II, JEOL, Tokyo, Japan) which was operated at 80 kV after dilution of 1 mL of the prepared F4-SLNs ten fold times with deionized water. After that, sonication for 10 minutes by means of an ultrasonic bath was performed. One drop of the diluted sample was drop-cast on the surface of a carbon-coated copper grid and dried for 5 minutes at room temperature. Finally, image capture and analysis using Digital Micrograph and Soft Imaging Viewer software were investigated.

### Scanning Electron Microscopy (SEM)

The surface morphology, shape and homogeneity of the drug, GMS lipid and the optimized SLNs were investigated using SEM (X-MaxN, JSM-6510LV, Oxford Instruments, UK). Mounting of the specimens with gold under low vacuum was performed prior to examination by means of a direct-current sputter coater to ensure superficial electro-conductivity of particles.<sup>25</sup>

## Fourier-Transform Infrared Spectroscopy (FT-IR Spectroscopy)

Spectra of MZL, GMS, Tween 80, their physical mixture corresponding to the optimized formula, freeze-dried F4, and its plain SLN were obtained by the aid of FT-IR spectroscopy (Thermo Fisher Scientific iS10 Nicolet).



Small samples (2 mg) were incorporated with potassium bromide. Then, they were ground into fine powder and pressed into KBr disks with a hydrostatic press. The scanning range was 500 to 4,000  $\text{cm}^{-1}$ .

## Differential Scanning Calorimetry (DSC)

Around 10 mg samples of each of MZL, GMS, and physical mixtures with the same ratio of the chosen formula. Freeze-dried F4 and its plain SLNs were held in standard aluminum pans of (Shimadzu DSC 50, Tokyo, Japan) and heated over a range (35°–300°C) at a heating rate of 10°C/min under a constant dry nitrogen atmosphere, purging at a flow rate of 20 mL/min.<sup>62</sup>

## X-Ray Diffractometry (XRD)

Any changes in the crystallinity of the compounds before and after formulation was investigated by XRD analysis using (Rigaku Rint-2500VL, Tokyo, Japan). X-ray diffractograms of MZL, GMS, physical mixture corresponding to the optimized formula, in addition to freeze-dried SLNs of the optimized F4 and its plain SLNs were achieved via X-ray diffractometer equipped with Cu-K $\alpha$  radiation at 3°–50°C at 2 $\theta$  angle under 45 kV voltage and 9 mA current.<sup>51</sup>

## Preparation of MZL-SLNs Based Hydrogels

MZL-SLNs (F4) composed of blends of lipid (GMS) weighing 400 mg (0.08%) and with 0.5% w/v Tween 80 as a stabilizer were selected for optimal formulae with small particles, low PDI, and high ZP and EE %.

Hydrogel was introduced for obtaining the viscosity levels suitable for topical ocular application. Briefly, a gelling mixture (1.5% w/v Na alginate with 5% w/v PVP K<sub>90</sub>) was well dispersed in distilled water with the addition of propylene glycol (10% w/v) as a plasticizer. Then, the appropriate weight of the lyophilized MZL-SLNs equivalent to 1 mg MZL/g hydrogel and the same weight of plain lyophilized SLNs were mixed with a homogenizer to obtain medicated and plain hydrogels, respectively.

The dispersion was neutralized with NaOH-solution drops, adjusting the pH value to 6.5–7 under mild stirring. Methyl paraben and propyl paraben (ratio 1:1) were used as preservatives (0.1% w/v). The final prepared hydrogel containing 0.1% w/v MZL was left overnight without stirring to get rid of any air bubbles. The drug-loaded SLNs hydrogel formula was stored at 2°–8°C until use.

The same protocol was used for preparation of blank hydrogels as negative (no treatment) controls.

## In Vitro Drug Release Studies

In vitro release of MZL from the freshly lyophilized medicated SLNs (F4) was studied. Specific weights (1 g) of the prepared hydrogels were uniformly spread over a modified vertical Franz diffusion cell of a diameter 2.5 cm, in addition to an aqueous suspension (as a control). In vitro release of blank hydrogel containing free drug was also considered. A dialysis membrane having a molecular weight cutoff between 12,000–14,000 Dalton was utilized and tightly involved between the donor and receptor compartments.

The receptor chamber contained 70 mL release medium composed of phosphate buffer pH 6.8 containing 0.5% w/v SLS. The dialysis membrane was soaked overnight in the release media before mounting it into the diffusion cell. Franz diffusion cells were placed in a GFL shaking incubator (Gesellschaft für Labortechnik, Burgwedel, Germany) maintained at 37°±0.5°C and continuously stirred at 100 rpm during the entire experiment. Lyophilized plain SLNs and medicated F4- SLNs containing the equivalent of 1±0.12 mg MZL were suspended in distilled water and sonicated, then placed in the donor compartment. Aliquots (2 mL) of the dissolution media were withdrawn at different intervals up to 36 hours, filtered through a 0.45  $\mu\text{m}$  Millipore filter, then replenished with fresh medium in order to maintain the sink condition throughout the experiment. Also, free MZL suspension experienced the same procedures to be used as a control.

The samples were extra-analyzed for drug concentration by the spectrophotometer at 230 nm. Each experiment was completed in triplicate, and the cumulative MZL released % was calculated at each time interval.

## Release-Data Analysis

In order to define the release kinetics of the drug from the SLNs and its prepared hydrogel, in vitro release data were fitted mathematically using the kinetic equations such as; zero order, first order, Higuchi diffusion, and Korsmeyer–Peppas semiempirical models. The choice of the superior mathematical model was dependent on the kinetic release profile that conveying the highest coefficient of determination ( $R^2$ ) using GraphPad Prism software version 6. Each experiment was run in triplicate and the mean were employed.

## Physical Stability of Optimized MZL-SLNs

The physical stability of the optimized formula (F4) was estimated under diverse storage conditions using International Conference for Harmonisation (ICH) guidelines.<sup>27</sup>

MZL-loaded SLNs aqueous dispersions (F4) were freshly prepared, lyophilized, and stored in amber-glass vials that were perfectly sealed, wrapped in aluminum foil, and maintained at refrigerated ( $4^{\circ}\pm 1^{\circ}\text{C}$ ) and ambient ( $25^{\circ}\pm 2^{\circ}\text{C}$ ,  $60\%\pm 5\%$  relative humidity) temperatures without any movement for 6 months. The stability of the selected formula was assessed after redispersion of freeze-dried F4 powder, with parameters measured being physical appearance, PS, distribution, surface charge, and EE % at time 0 (initial), and after 1, 2, 3, 4, 5, and 6 months of storage. Plain SLNs were prepared and utilized as controls.

## Ocular Irritation Testing

The Draize test is the most reliable method for determining ocular irritation from plain and MZL-SLNs containing sodium alginate/PVP K<sub>90</sub> hydrogels.<sup>20</sup> This optimized ophthalmic formula was selected according to in vitro drug release and stability data. All animal work was approved by the Ethical Committee of the Faculty of Pharmacy, Mansoura University, Egypt in accordance with the guidelines outlined in the *Guide for the Care and Use of Laboratory Animals* (NIH publication 85-23, revised in 1985). Seven New Zealand male albino rabbits were subjected to the administration of the optimized formula in order to evaluate the degree of irritation. Draize test uses a scoring system ranging from 0 (no irritation) to 3 (highest irritation and redness) for the cornea, iris, and conjunctivae. The tested formula was applied in the conjunctival sac of the right eye, and the left eye was kept as control by instillation of saline. The cornea, iris, and conjunctiva were examined for any signs of irritation or congestion caused by the formulation. Testing the ocular irritation score was done at intervals of 1, 2, 5, 8, and 24 hours after administration.<sup>50</sup>

## Induction of Congestion in Rabbits' Eyes

The induction of conjunctivitis in rabbits' eyes was made by ocular instillation of a histamine solution in a concentration of 1% (w/v).<sup>45</sup> Two drops of the solution were instilled into the two eyes of each rabbit. One of the eyes served as a test using the tested ophthalmic formulation

and the second as control using saline drops. The eyes were examined every 5 minutes until maximum hyperemia, which was developed after 30 minutes of histamine solution instillation.

## Treatment of Allergic Conjunctivitis

The experimental procedures obeyed the ethical principles of the Scientific Committee of the Faculty of Pharmacy, Mansoura University, Egypt for the use of experimental animals. Four groups of male albino rabbits (six in each group) weighing 2.0–2.5 kg were used. The rabbits were subjected to normal feeding, ventilation, and illumination. For each animal, one of the inflamed eyes served as a test and the second as control. An appropriate weight of each formula equivalent to 0.1 mg MZL was applied to the tested eye, while 100  $\mu\text{L}$  of saline drops were used in the other eye. Treatment with MZL-loaded gel formula was done 30 minutes from the histamine solution instillation (maximum redness).

## Tested Formulations

Four groups (n=6 per group) were divided as follows:

- Group I: normal untreated negative control (phosphate buffered saline (PBS drops))
- Group II: positive control (histamine solution)
- Group III: treatment with free MZL containing sodium alginate/PVP K<sub>90</sub> hydrogel compared to plain hydrogel
- Group IV: treatment with MZL- SLNs containing sodium alginate/PVP K<sub>90</sub> hydrogel compared to plain hydrogel

## Ophthalmological Examination of Rabbits' Eyes

Observations were made every 5 minutes for complete removal of the eye redness throughout the study after the application of the selected formulations. Corneas were examined with a magnifying lens. In addition, the gross appearance of control and tested eyes was photographed.

## Histopathological Examination

The aim of this study was to assess the effects of topical ocular MZL in an animal model of allergic conjunctivitis in albino New Zealand rabbits, which were divided into six groups:

- Group I: normal untreated negative control (PBS drops)
- Group II: positive control (histamine solution)
- Group III: post-treatment with free MZL-loaded 1.5% w/w sodium alginate/5% w/w PVP K<sub>90</sub> hydrogel
- Group IV: post-treatment with MZL-SLNs-loaded 1.5% w/w sodium alginate/5% w/w PVP K<sub>90</sub> hydrogel
- Group V: pre-treatment with free MZL-loaded 1.5% w/w sodium alginate/5% w/w PVP K<sub>90</sub> hydrogel
- Group VI: pre-treatment with MZL-SLNs-loaded 1.5% w/w sodium alginate/5% w/w PVP K<sub>90</sub> hydrogel

The animals from each group were sacrificed and conjunctival specimens were dissected and immediately immersed in neutral buffer formalin 10% for fixation. After 24 hours, the samples were washed, dehydrated, and cleared. Sectioning of paraffin-embedded tissue by microtome to 5  $\mu$ m was done and stained with hematoxylin and eosin (H&E) to be further examined using light microscopy. Counting of eosinophils, plasma cells, and apoptotic cells in four squares of 1  $\mu$ m diameter each per high-power field were counted. The thickness of the covering epithelium of the eyelids was measured with a Java-based image-processing program (ImageJ analysis).

## Immunohistochemical Staining for Localization of TNF- $\alpha$ and VEGF

Paraffin blocks of separated conjunctivae were sectioned and immersed in clearing agents and then passed through serial alcohol concentrations. After that, immunohistochemistry protocol for VEGF and TNF- $\alpha$  paraffin blocks was investigated by antigen retrieval by the aid of heating in acetic acid (pH 6.0). This was followed by blocking of endogenous peroxidase by H<sub>2</sub>O<sub>2</sub> (3%) for 10 minutes.

Incubation with primary antibodies against TNF- $\alpha$  and VEGF rabbit polyclonal antibodies, ready to use, overnight at 4°C was completed. Then, tissue samples were washed three times with PBS, accompanied by the addition of anti-rabbit secondary antibodies for 1 hour. Labeling was visualized by incubation with DAB chromogen at room temperature for 5 minutes. This is utilized in many applications for visualization of peroxidase activity. In the peroxidase reaction, DAB serves as a hydrogen donor in the presence of peroxide. The oxidized DAB

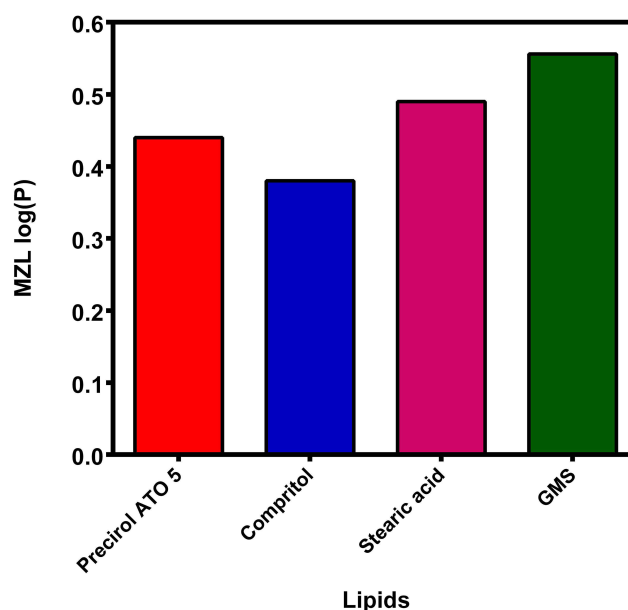


**Figure 1** Determination of drug-partition coefficient using different lipids.

**Abbreviations:** MZL, mizolastine; GMS, glycerylmono stearate; P, partition coefficient.

forms an insoluble brown end product for use in immunohistological and immunoblotting staining procedures. Finally, the sections were subsequently counterstained with H&E. Immunopositive cells per 1,000 were counted by using ImageJ.<sup>19</sup>

## Statistical Analysis

Statistical analysis was employed utilizing one-way ANOVA followed by Tukey–Kramer multiple-comparison tests, as well as Student's *t*-test for stability study and comparison of different groups. Student's *t*-test was also used to compare different groups using GraphPad Prism software version 6 at  $P < 0.05$ . All the results were given as means  $\pm$  SD.

## Results and Discussion

### Lipid Selection for SLNs

Based on partition-coefficient measurements of the drug, GMS ( $\log P = 0.55 \pm 0.11$ ) was chosen as the lipid base for preparation of MZL-SLNs (Figure 1). Its high biocompatibility and sustained-release profile of made it an excellent excipient for nanoformulation.

### Optimization and Characterization of MZL-SLNs

Hot homogenization is the preferred method to formulate SLNs overloaded with hydrophobic drugs, owing to its

**Table 2** Coded independent variables and properties of MZL-loaded SLNs prepared according to 3<sup>2</sup> full factorial design

Formula	Independent variables		Dependent variables (mean ± SD)			
	Code of (A)	Code of (B)	MPS (nm)	PDI	EE (%)	ZP (mV)
F1	+I	+I	287.66±4.13	0.30±0.02	38.1±2.35	-21.1±1.2
F2	+I	0	296.2±2.03	0.24±0.04	53.0±3.35	-26.03±3.35
F3	+I	-I	500.07±10.6	0.34±0.14	88.5±0.71	-16.4±1.80
F4	0	0	185.36±2.56	0.26±0.01	86.5±1.47	-22.03±3.65
F5	0	+I	199.03±0.91	0.36±0.04	29.2±6.28	-12.1±1.90
F6	0	-I	353.23±39.1	0.087±0.04	66.4±0.75	-15.6±1.55
F7	-I	+I	172.53±1.77	0.313±0.03	56.99±3.73	-10.8±0.46
F8	-I	0	213.06±2.65	0.30±0.026	80.8±1.47	-11.6±1.85
F9	-I	-I	460.5±33.5	0.195±0.14	75.8±2.46	-13.9±1.29

**Abbreviations:** MPS, mean particle size; PDI, polydispersity index; ZP, zeta potential; EE, entrapment efficiency; A, lipid amount variable; B, surfactant concentration variable.

relative simplicity, efficiency, and enhanced EE, thus being used in about 50% of the reported investigations.<sup>27</sup>

We observed that after the addition of sodium chloride, PS growth during centrifugation have increased and consequently the efficiency of centrifugation, along with entrapment of the drug inside the SLNs. This was interpreted due to the fact that NaCl had a significant effect in the case of vesicles, provided its concentration were sufficiently high (>50 mM), which expected to be related primarily to osmotic pressure.<sup>53</sup>

SLNs have several characteristics, such as good drug-loading capacity and the capability of entrapping both hydrophilic and hydrophobic substances with numerous properties, delivering drugs at defined rates and thus enhancing their intracellular uptake. By means of lipids, vesicles are being used as simplified models of cells and biological membranes. Their similarity to biomembranes makes them an ideal structure, not only for the study of existing biosystems but also in the investigation of the emergence, functioning, and evolution of original cells.<sup>13</sup>

Minimum PS, smallest PDI, maximum EE %, and reasonable ZP are vital requirements and should be kept in consideration for enhancing the drug absorption and subsequently its bioavailability.

In terms of the full factorial design, the dependent variables MPS, PDI, EE, and ZP were taken as signs of the reproducibility and efficiency of the processing technique. From the data and parameters of factorial design for F1–F9, polynomial equations for our four dependent variables were proposed and discussed (Table 2).

## Analysis of MPS and PDI

Not only the average PS (nm) of SLNs is principal, but also their PDI values which are measure of PS distribution.

Therefore, these two essential criteria of NPs influence drug release rate, bio-distribution as well as bioavailability. As lipid carriers larger than 100–150 nm can be taken up by phagocytes or remain in tissues for an extended time.<sup>13</sup> Danaei et al 2018, highlighted the significance of size and PDI in the successful design, formulation and development of nanosystems for pharmaceutical, and other applications.

The PS of MZL-SLNs ranged from 172.53±1.77 nm to 500.07±10.6 nm which is primarily suitable for ocular delivery while, PDI values ranged from 0.087±0.04 to 0.36±0.04 as overviewed in (Table 2). The small values of PDI describe narrow-distribution for PS and offer a homogenic suspension. Also, they are wanted to preserve the colloidal dispersion stability devoid of microparticulates or precipitates development.

In the model fit for PS, *P* values suggested “quadratic model” for MPS analysis which maximizing the Adjusted R<sup>2</sup> and the Predicted R<sup>2</sup> however, linear model is suggested for PDI as if there are many insignificant model terms, model reduction may improve that model.

Equations 4 and 5 display the quantitative effect representing the regression model of formulation components (independent variables A and B) on response parameters (Y1 and Y2), in the form of their equivalent polynomial equations and regression coefficients for MPS (Y1) and PDI (Y2) as follows:

$$MPS(Y1) = +181.23 + 37.63A - 109.94B + 19.31AB + 75.68A^2 + 97.04B^2 \quad (4)$$

$$PDI(Y2) = +0.26 + 0.002A + 0.067B \quad (5)$$

The coded equation is beneficial for detecting the relative impact of the factors by comparing the factor coefficients.



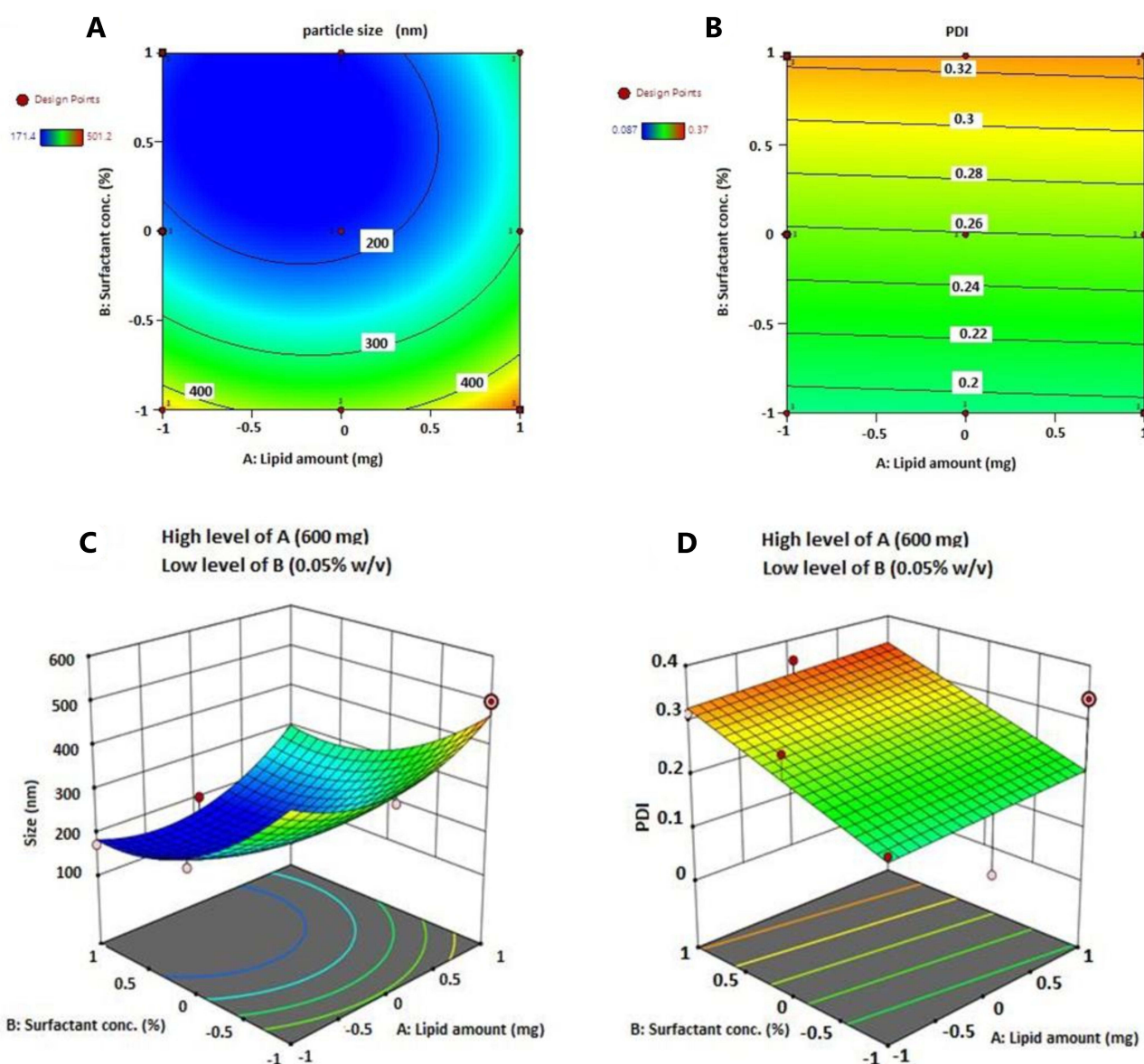


**Figure 2** Contour (**A and, B**) and three-dimensional surface (**C and, D**) plots displaying the effect of the interaction between the amount of lipid (**A**) and surfactant concentration (**B**) upon particle size and PDI.

The equation in terms of actual factors can be utilized in making predictions about the response for given levels of each factor. A coefficient with positive sign represents a positive consequence. It has been noticed that, by increasing the concentration of lipid (A) in the dispersion, generally larger particle sizes are attained. The largest MPS obtained ( $500.07 \pm 10.6$  nm) at high level (+1) of A and low level (−1) of B from batch F3.

Lipid concentration was the major factor affecting positively the above two responses, when increasing GMS (A) from 300 mg to 600 mg and keeping B constant, PS and PDI increased (Table 2). Similarly, the interaction

term AB, ie when lipid and surfactant were increased together, caused moderate increase in the MPS which may be due to the existence of lipid in comparatively higher amounts denoting a synergistic effect upon PS.

The increase in the PS with increasing the amount of lipids (A) may be due to the aggregation of more particles, resulting in larger PS as they increase the viscosity and decrease the rate of the diffusion into the aqueous phase leading to the formation of nanoparticles with higher size or lipid aggregates.<sup>15</sup>

On the other hand, the concentration of Tw 80 (B) experienced a negative effect on PS however, experts a negligible positive effect on PDI. As the surfactant



concentration increased from 0.25% to 1% w/v, better stabilization of the smaller lipid droplets was permitted by reducing interfacial tension between the organic phase and aqueous phase through formation of a steric barrier on the particle surface, and thereby protect smaller particles and prevent their coalescence into bigger ones. Accordingly, effective formation of a stable emulsion with smaller and uniform droplet size nanoparticles with low polydispersity is manifested.<sup>22,31,36</sup>

The correlation between the dependent and independent variables was extra clarified using response-surface and contour plots. Figure 2 shows contour plots and 3D response surface plots for MPS and PDI, respectively, illustrating the influences of independent variables A and B on both response parameters.

## Entrapment Efficiency

This critical quality attribute (CQA) is an appropriate way used to judge the effectiveness as well as reproducibility of the processing technique. The EE% of the prepared SLNs ranged from 29.2±6.28 to 88.5±0.71%. The obtained polynomial equation for EE (%) is expressed as follows:

$$EE\% (Y3) = +71.24 - 6.08A - 17.12B - 6.34AB + 3.99A^2 - 16.76B^2 \quad (6)$$

Upon careful examination of the previous equation, we conclude that both concentration of lipid (A) the surfactant concentration (B) had negative effect on EE%. A considerably increase in entrapment of MZL was reached at low level (-1) of A (300 mg) and low level of B (0.25%) as in batch F9 (75.8±2.46%).

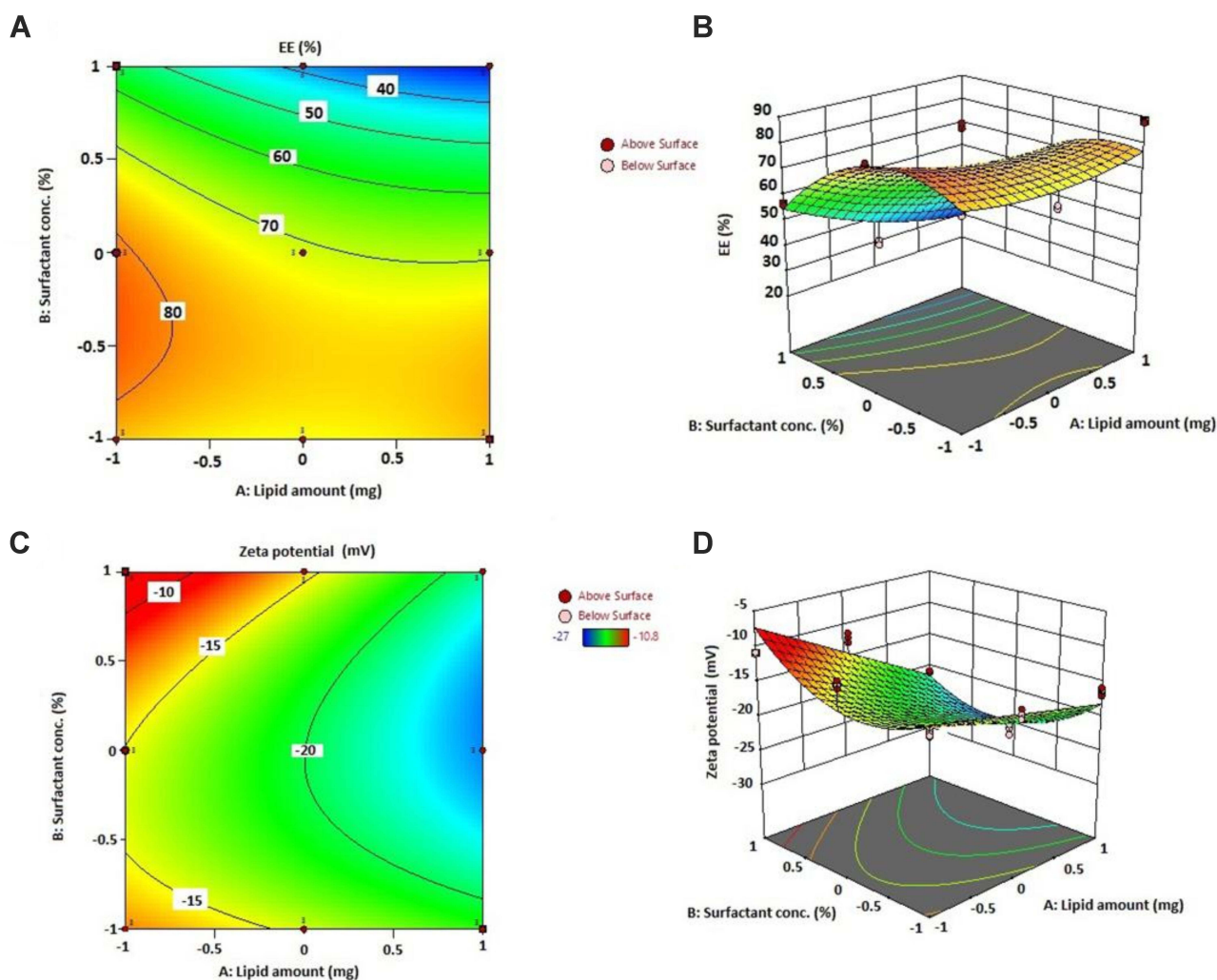


**Figure 3** Contour (A and, C) and three-dimensional surface (B and, D) plots showing the effect of interactions between the amount of lipid and surfactant concentration on entrapment efficiency and zeta potential, respectively.

**Table 3** ANOVA results for responses

Responses	Source	F value	P value	Inference	Adjusted R <sup>2</sup>	Predicted R <sup>2</sup>	Adequate precision
Particle size (Y1)	Quadratic	108.81	<0.0001	Significant	0.9608	0.9330	24.02
PDI (Y2)	Linear	9.31	0.0014	Significant	0.4302	0.1551	5.54
EE% (Y3)	Quadratic	11.87	<0.0001	Significant	0.7118	0.5391	8.28
ZP (Y4)	Quadratic	16.96	0.0008	Significant	0.7839	0.6212	12.95

**Abbreviations:** PDI, polydispersity index; ZP, zeta potential; EE, entrapment efficiency.

Crystallization is strongly connected with drug incorporation and higher degree of crystallization reduces drug entrapment in SLNs and vice versa. This may be interpreted the effect of GMS on EE% as this lipid type is one of lipids which form highly crystalline particles with a perfect lattice leading to drug expulsion especially at higher concentrations so the crystalline lattice of GMS which prevents more efficient entrapment of the drug in nanoparticles.<sup>22</sup> Another explanation was that, an augmented lipid concentration had a positive effect on drug solubility within the lipid core with significant increase in mixture viscosity.<sup>30</sup>

To make the interpretation of the influence of different CPP on the CQAs easier, the model equations for different CQAs were used to create several graphical plots. Figure 3A and B show the contour plots and three-dimensional (3D) response surface plots of EE.

It was revealed by the model graphs that the gradual increase in the concentration of surfactant from 0.25 to 1% w/v resulted in an ongoing decrease in the EE of SLNs formulations (Figure 3A). The higher value of the B coefficient (17.12) specifies that the surfactant concentration is the major aspect that affects EE%. This observed decline in EE could be clarified by partition phenomenon. High surfactant level in the external phase might increase the partition of drug from internal to external phase due to the increased solubilization of the drug in the external aqueous phase so extra amount of drug can diffuse and dissolve in it.<sup>36</sup>

This was confirmed in our design as formulations contain relatively high amounts of surfactant such as (F1 and F5) exhibited better leakage and consequently decrease in EE% which possibly due to a reduction in interfacial tension imparted by the rise in surfactant concentration.

Amongst all the tested batches, the optimum PS with maximum % EE was achieved in batch F4, formulated with mixture of medium level of A (400 mg) and medium level of (B) (0.5%).

## Zeta Potential

The chemistry of the particles and the extent of repulsion between similarly charged ones in the nanodispersion have a major influence on the polarity. Usually, higher positive or negative ZP values are necessary for SLNs as the similar charges produce electrostatic repulsion and thereby prevent the aggregation of particles. Such a criterion is broadly helpful in prediction the colloidal suspension stability.<sup>54</sup>

In this design, SLNs enclosed by a non-ionic surfactant like Tw 80 have a tendency to persist stable regardless of having a relatively low value of ZP. That shield of SLNs with surfactant reduces the electrophoretic mobility of the particles by steric stabilization and thus lowers the ZP.<sup>48</sup> In case of F4, ZP of about −22 mV, is still satisfactory to entirely stabilize the system.

The obtained polynomial equation symbolizing the regression for ZP model is as follows;

$$ZP(Y4) = -19.97 - 4.88A + 0.54B - 2.19AB - 0.014A^2 + 5.05B^2 \quad (7)$$

The ZP of all the prepared formulae was regularly negative and in the range of −10.8±0.46 to −26.03±3.35 mV (F7 and F2, Table 2). The polynomial equation revealed that the lipid amount has negative coefficient concerning ZP with a somewhat low numerical values while surfactant concentration had a positive effect.

The contour and three-dimensional (3D) response surface plots (Figure 3C and D) revealed that the ZP was highest at high level of lipid (A) when intermediate level of surfactant (B) was used. Furthermore, the lowest ZP value was obtained at higher levels of A and B.

The regression analysis results for all the four responses (Y1, Y2, Y3 and Y4) are summarized in Table 3. The “Predicted R<sup>2</sup>” values for all the dependent variables were found to be in reasonable agreement with the “Adjusted R<sup>2</sup>” values.

The regression model equations prove that, the response Y1 (MPS) was significantly affected by the

**Table 4** Adjusted levels of independent variables and predicted and observed responses for optimized formula

Optimized formula coded level	Optimized actual value	Responses	*Predicted mean value	Observed experimental value
Lipid amount [0]	400 (mg)	Y1 particle size	181.009 nm	185.36±2.56 nm
		Y2 PDI	0.258	0.26±0.01
Surfactant concentration [0]	0.5 (%)	Y3 EE (%)	71.91%	86.5%±1.47%
		Y4 ZP	-19.97 mV	-22.03±3.65 mV

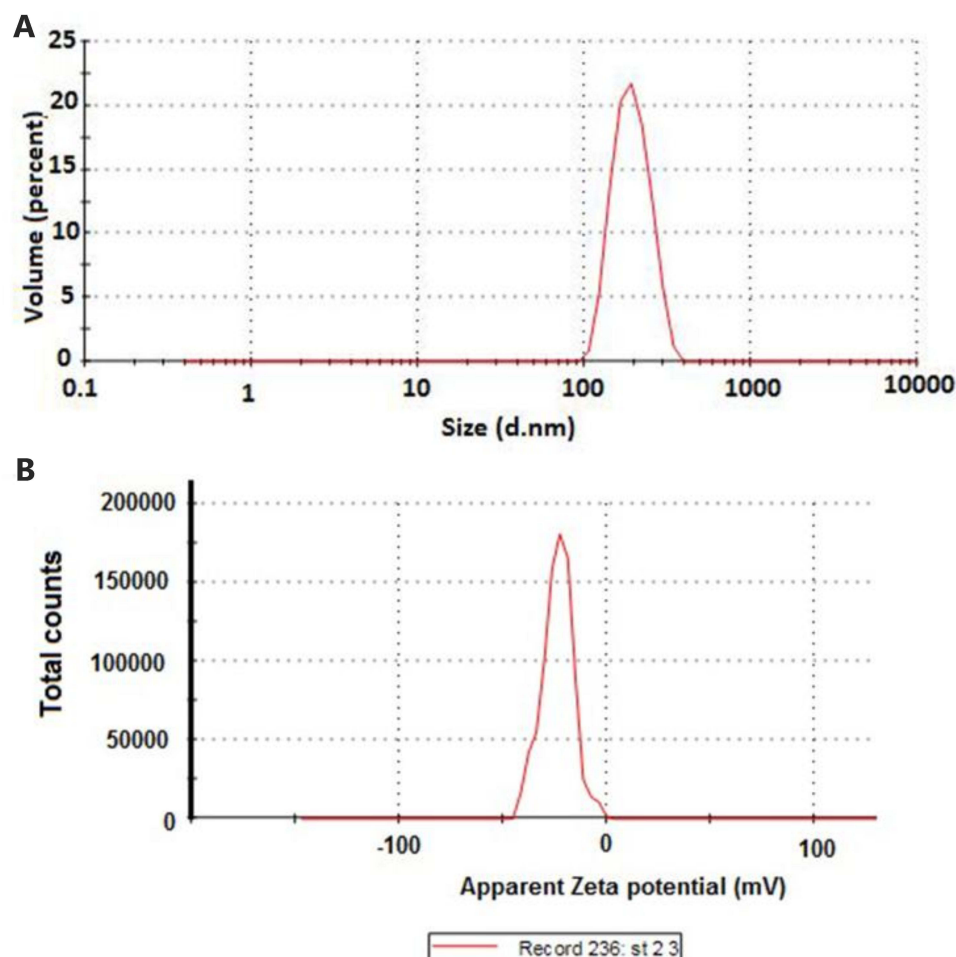
**Note:** \*Point prediction at confidence of 95% and population of 99%.

**Abbreviations:** PDI, polydispersity index; ZP, zeta potential; EE, entrapment efficiency.

positive effects of quadratic contribution of all model terms (A, B, AB,  $A^2$  and  $B^2$ ). While, Y2 (PDI) was negatively affected by the linear contributions of both factors (A) and (B). The response Y3 (EE%) was significantly affected by the positive effects of quadratic impact of the factor B besides A, B and  $B^2$  are significant model terms, whereas the response Y4 (ZP) was significantly

influenced by the positive effects of quadratic involvement of the terms A, AB and  $B^2$ .

The response surface models were tested with ANOVA. The model *P* value was < 0.05 level of significance signifying that, the predicted model could well describe the relationship between the independent and dependent variables.

**Figure 4** Representative (A) particle size–distribution graph and (B) zeta potential distribution of optimized MZL-SLNs.

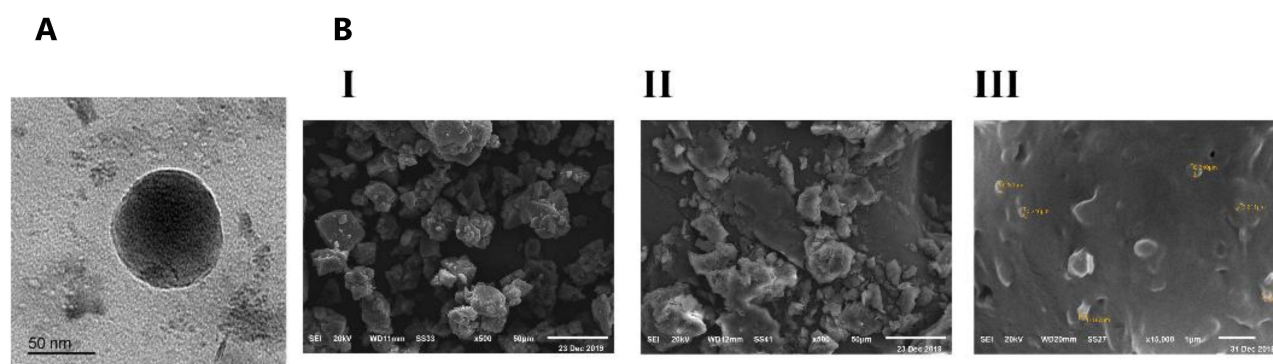


**Figure 5** Transmission electron microscopy of F4 -SLNs (A) and scanning electron microscopy (B) images of (I) MZL, (II) GMS lipids, and (III) F4- SLNs.

Adequate precision measures the signal to noise ratio. A ratio greater than 4 is desirable. This model can be used to navigate the design space.

Based on the Design Expert Version 12.0.9.0, Response Surface (Study Type) User Defined design type and a desirability factor of 88.2%, for optimization with prediction goal fixed at minimized (PS and PDI) and maximized (EE% and ZP), the optimized formula F4 with (A [0] and B [0]) denoted the highest EE% besides low PS and PDI was obtained. The optimized MZL-SLNs was prepared with the optimized level of component and process variables summarized in Table 4.

The investigational values of PS, PDI, EE, and ZP of the optimized F4 were established to be  $185.36 \pm 2.56$  nm,  $0.26 \pm 0.01$ ,  $86.5 \pm 1.47\%$  and  $-22.03 \pm 3.65$  mV, respectively. This SLNs formula will be subsequently subjected to further evaluations. Figure 4 represents a PS-distribution graph and ZP distribution of optimized MZL-SLNs.

## Transmission Electron Microscopy (TEM)

The size, shape, and surface morphology of nanoparticles were visualized by transmission electron microscopy (TEM) (Figure 5A). MZL-SLNs were uniform in size and morphology, showed small particle in nano-sized diameter and spherical shape with a lipid core enriched with the drug and shell of surfactant.<sup>9</sup>

## Scanning Electron Microscopy (SEM)

As apparent from Figure 5B, the particles of F4 are spherical and regular in shape with smooth surfaces and uniform distribution. There was a distant spread the particles

because of the lipid nature of carriers and sample preparation before SEM analysis.<sup>6</sup>

## Fourier-Transform Infrared Spectroscopy (FT-IR)

FT-IR helps us to confirm the identity of MZL and to detect the drug interaction with other components.

The infrared spectrum of MZL is specified in (Figure 6A (I)) indicating distinctive peaks at  $3054 \text{ cm}^{-1}$  (C-H arom.),  $2845\text{--}2933 \text{ cm}^{-1}$  (C-H aliph.),  $1511\text{--}1559 \text{ cm}^{-1}$  (aromatic rings),  $1011 \text{ cm}^{-1}$  (C-N), ( $3316\text{--}3417 \text{ cm}^{-1}$ ) peaks corresponding to N-H stretching vibration and  $1678 \text{ cm}^{-1}$  depicted C=O stretching.

The FT-IR spectrum of GMS (II) showed the existence of characteristic IR peaks at  $2851\text{--}2919 \text{ cm}^{-1}$  that may be linked to the carbon-hydrogen stretch in the -CH<sub>2</sub> alkane groups present in the acyl chain of the fatty acid. However, the beak at  $1179 \text{ cm}^{-1}$  is related to C-C stretch coupled to CH<sub>2</sub> and the peak at  $1438 \text{ cm}^{-1}$  for (C=C). The wave number at  $1735 \text{ cm}^{-1}$  is attributable to C=O stretching vibration related to carboxylic group.<sup>46</sup>

Tw 80 spectrum (III) displayed an absorption band at  $2920 \text{ cm}^{-1}$  of methyl group (-CH<sub>3</sub>), while the band at  $2864 \text{ cm}^{-1}$  was due to -CH<sub>2</sub>-stretching. The band at  $1735 \text{ cm}^{-1}$  could be attributed to C=O.

The spectrum of physical mixture of F4 (IV) demonstrated the summation bands of the drug and other components with reduced intensities as a consequence of dilution effect. The IR spectrum of lyophilized drug-loaded SLNs (VI) showed the absence of the distinctive absorption bands of MZL. This may be a reflection to the drug entrapment inside the lipid matrix. These results were in agreement with,<sup>51</sup> who interpreted the absence of the drug peaks as a result of better chance for efficient



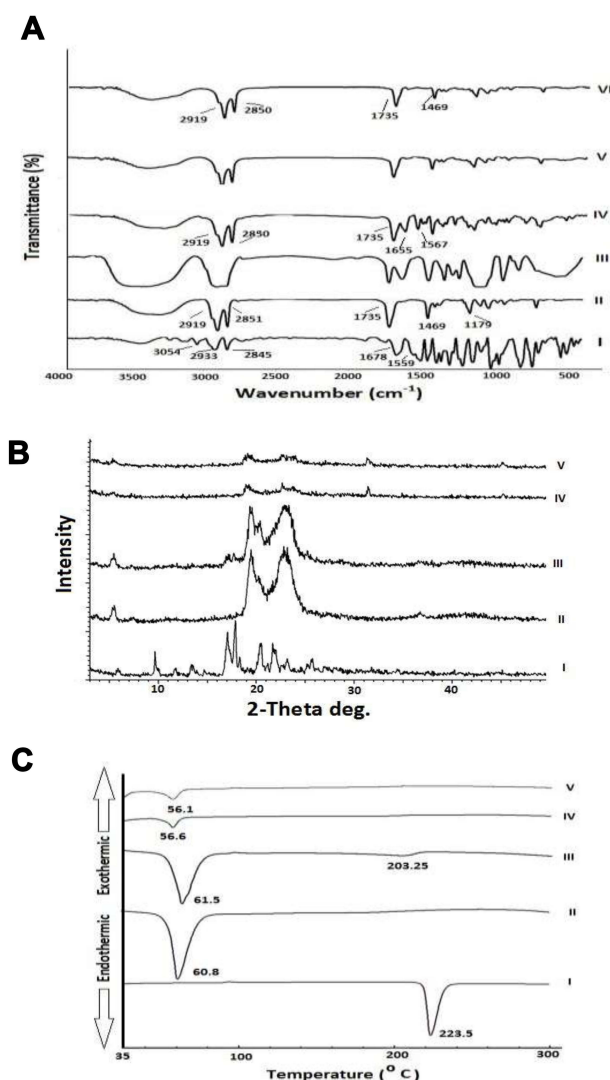


**Figure 6** Solid characterizations.

**Notes:** (A) FTIR spectra, (B) XRD patterns, and (C) DSC curves of (I) MZL, (II) GMS, (III) Tween 80, (IV) physical mixture, (V) plain F4-SLNs, and (VI) drug-loaded F4-SLNs.

**Abbreviations:** GMS, glyceryl monostearate; FTIR, Fourier-transform infrared spectroscopy; DSC, differential scanning calorimetry; XRD, X-ray diffractometry.

incorporation of isoniazid in the free space generated between the disrupted fatty acid chains.

Based on the results of FTIR, it revealed that there was no significant interaction between the drug and lipid in SLN formula, and MZL was compatible with the applied FTIR excipients.

## Powder X-Ray Diffractometry (PXRD)

PXRD analysis is an exclusive method that permits the determination of the drug crystalline or amorphous state

and its crystal alterations.<sup>28</sup> The XRD patterns of MZL, GMS lipid, their physical mixture, plain F4-SLNs in addition to medicated one are presented in Figure 6B.

The XRD pattern of MZL (I) showed the principal peaks at angles; 17.9°, 18.36°, and 34.5° at (2θ) angle, representing the crystalline nature of drug. The reduction in crystallinity of GMS was also evaluated by XRD analysis (II) which had distinguishing peaks at angle 19.5°, 22.9°, and 36.7°(2θ). The physical mixture (III) preserved the characteristic peaks of both the drug and GMS.

Figure 6B (IV and V) illustrated a sharp decrease in intensity of the lipid peaks indicating the reduction in crystallinity of less ordered GMS crystals that were existed in both plain and drug loaded SLNs formulae.

The loss of crystallinity in the XRD pattern of the lyophilized MZL -loaded SLNs (F4) (V) was distinguished through the disappearance of sharp peaks and the loss of most distinctive peaks of the drug. These findings propose the entrapment of MZL within the lipid imperfections in an amorphous state. The change in crystallinity of lipid and drug would be expected to affect the release profile of drug from nanoparticles. The amorphous form is thought to have several characters such as higher energy with a superior surface area, subsequently, greater solubility, dissolution rates, and consequently improved bioavailability.<sup>28</sup>

As a result of the transformation of the drug crystallinity to an amorphous one or a disordered crystalline phase of a molecular dispersion and decreasing the crystalline status of lipid, deep-rooted our results of the suitable drug incorporation into SLNs. For the reason that, the less ordered lipid matrix favors the increasing number of voids in its structure. Thus, it is able to accommodate a larger amount of drug. This explanation is corroborated with that revealed by.<sup>8</sup>

## Differential Scanning Calorimetry Analysis (DSC)

DSC results signify the probable changes in crystallinity of the lipid after the addition of the drug and formulation as SLNs.

Figure 6C displays the DSC curves of the drug, GMS lipid, their physical mixture, plain F4-SLNs as well as medicated F4-SLNs.

The DSC thermogram of MZL (Figure 6C (I)) demonstrated a melting endothermic peak at 223.5°C which indicated the crystalline nature of pure MZL; this also



confirmed the XRD results. Figure 6C II showed distinctive sharp endothermic peak of GMS at 60.8°C. That sharp peak of bulk lipid clarified its crystalline nature.

The thermogram of their physical mixture (III) experienced only one sharp melting point corresponding to the bulk lipid (GMS) whereas, reduction of intensity of drug endothermic peak with shifting to lower temperature at 203°C which owed to the partial molecular dispersion of MZL in GMS during the run as the mixing of drug and excipient, which lowered the purity of each component in the mixture. This was similarly interpreted with,<sup>16</sup> who studied the decomposition of some drugs in well-defined thermal events, translating the suitability of thermal techniques for the characterization of the drug/excipients interactions.

Markedly, the melting point of the bulk lipid (GMS) was reduced after formulation as SLNs in both lyophilized plain SLNs (56.6°C) (IV) and MZL -loaded SLNs (56.1°C) (V). That decrease could be explained on the basis that, the phase transition temperature of colloidal dispersion was always much lower than that of the anhydrous lipid.<sup>2</sup> Another interpretation for the decrease in the melting point is that, the small PS of SLNs results in a high surface

energy, which creates an energetically suboptimal state that results in lowering the melting peak<sup>39</sup>.

The melting peak of MZL was disappeared in the thermograms of MZL-SLNs formulation that specified complete solubility or homogenous dispersion of the drug in the lipid matrix upon heating of lipid. As the crystal is more organized, less space is available for different molecules. These molecules attend to disturb the thermodynamically desired crystal ordering and accountable for higher drug entrapment.<sup>21</sup>

From DSC thermograms, no interaction between Mzl and GMS was distinguished.

## In Vitro Drug Release Study

In vitro release study has been completed up to 48 hours by means of modified Franz-diffusion cell to illustrate the mechanism of MZL release from SLNs. The in vitro release of MZL from the drug suspension alone (CL) and the selected MZL-SLNs F4 formula was done in phosphate-buffered pH 6.8 containing 0.5% w/v SLS at 37°C to retain the sink condition as shown in Figure 7.

In general, the release of drug from lipid-based colloidal systems was affected by several factors including; temperature and nature of the release medium, drug load and drug position in the particles, the dimension and contour of the particles, the crystalline arrangement of the drug and the lipids of the matrix, the nature of the stabilizing agents and their organization around the particles and the manufacture method of the nanoparticles.<sup>26</sup>

Free MZL diffusion reached  $66.5 \pm 2.5\%$  at nearly 8 hours at and approximately complete drug was released within 24 hours. On the contrary, the release profile of MZL from SLNs possessed a biphasic pattern, including a burst and a sustained drug release that was essential to prolong the retention time of the drug and ensure good efficacy. It was fast approximately  $43.7 \pm 1.3\%$  was released within 8 hours monitored by a slower and continuous release attaining  $71.3 \pm 2.3\%$  throughout 30 hours.

This biphasic release behavior may be linked to the fact that, the presence of the hydrophobic long chain fatty acids in the lipid forming SLNs hinders the drug release as a result of the essential for the drug to be released from the core-shell nanometer structure instead of being directly exposed to the release medium and consequently, more sustained release pattern is obtained.<sup>40</sup>

The initial burst effect could be related to the short diffusion path of the drug portion positioned on the outer

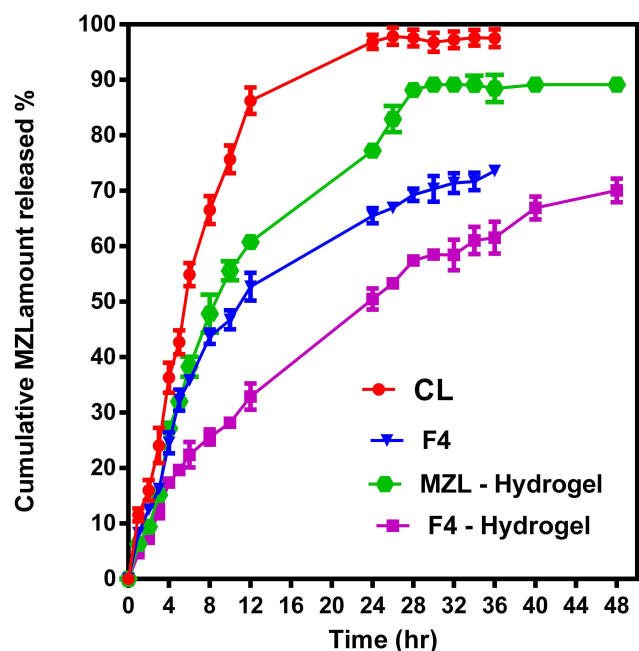


**Figure 7** In vitro release profiles of control mizolastine suspension (CL), optimized F4-SLNs, 0.1% w/v MZL-hydrogel, and F4 hydrogel formulae in phosphate buffer pH 6.8 containing 0.5% w/v SLS.

**Notes:** Data expressed as means  $\pm$  SD (n=3); SLS, sodium lauryl sulfate; SLNs, solid-lipid nanoparticles.

**Table 5** Kinetic release models of free mizolastine (CL) and SLN-F4 formula at pH 6.8 containing 0.5% w/v SLS

Formula code	Coefficient of determination			Korsmeyer–Peppas			Main transport mechanism
	Zero-order	First-order	Higuchi model	R <sup>2</sup>	N	K	
CL	0.8040	0.9770	0.9299	0.9446	0.77	1.0	Non-Fickian
SLN-F4	0.8766	0.9554	0.9680	0.9457	0.55	0.99	Non-Fickian

**Notes:** CL, free mizolastine suspension (control); N, diffusional exponent indicative of the mechanism of drug release (slope); K, intercept.

shell of the SLNs. These results are correlated well with,<sup>49</sup> who proposed that, the burst effect of ciprofloxacin was due to the rapid dissolution of drug molecules that are on the surface of the SLNs.

The second phase of slow release can be explained as, MZL was dispersed and entrapped uniformly into the lipid matrix and it can only be released from it through slow dissolution and diffusion.

It was reported in a study by<sup>14</sup> that, the PS has a direct influence on the drug release profile as the smaller particles has a larger surface area exposed to release media that principal for the high initial burst release effect.

Meanwhile, MZL-SLNs dispersed in gels produce minimal burst release of drug. A minimization of such initial burst and slower long-term drug release may be attributable to diffusional resistance of the gel in a semi-solid matrix as well as adhesion properties of the polymeric gel structure. Moreover, the thickness of the diffusion boundary layer limits the release of drug molecules into the aqueous buffer.<sup>63</sup> However, the drug release percent was 89.13±1.03% and 70.07±2.1% for MZL- and F4- hydrogels, respectively within 48 hours. This may be attributed to the diffusion of drug from the SLNs surface and thereafter from the core.

## Kinetic Analysis and Mechanism of Drug Release

Drug release data were fitted to different kinetic models. Fitting parameters such as correlation coefficients (R<sup>2</sup>) and the exponent “n” for Korsmeyer–Peppas equation were demonstrated in Table 5.

The data presented a better fitting to Higuchi model as the R<sup>2</sup> value was comparatively greater than that of other kinetic models which are 0.9164 and 0.9680 for the CL and SLN-F4, respectively.

Korsmeyer–Peppas was shown to be the most appropriate model to further analyze the release of matrix-based pharmaceutical dosage forms. It is required when the release mechanism is not obvious or when more than one release phenomena could be involved.<sup>33</sup>

The values of release exponent, n, observed using Peppas model were found to be 0.5 ≤ n ≤ 0.89, which elucidated that, the release profile was a pairing of diffusion and erosion mechanisms (anomalous non-Fickian transport).<sup>42</sup>

Additionally, the drug pointed to “n” value closer to 0.5, which displayed mainly diffusional drug release. Briefly, drug release from polymer matrix was diffusion controlled process rather than polymer erosion. These results were found to be in agreement with those obtained by.<sup>49</sup>

**Table 6** Stability data for MZL-SLNs (F4) after storage at two different temperatures

Storage time	Evaluation parameters							
	Refrigeration temperature (4°±1°C)				Room temperature (25°±2°C)/60%±5% RH			
	MPS (nm)	PDI	EE (%)	ZP (mV)	MPS (nm)	PDI	EE (%)	ZP (mV)
Initial	202.3±13.59	0.26±0.01	86.5±1.47	-22.03±3.65	202.3±13.59	0.26±0.01	86.5±1.47	-22.03±3.65
1 month	202.2±16.46	0.271±0.02	85.50±4.86	-21.66±0.93	189.4±9.72	0.220±0.26	87.37±4.14	-22.20±1.67
2 months	210.23±9.66	0.272±0.010	86.23±3.43	-20.73±2.25	187.13±3.6	0.267±0.064	85.43±4.67	-24.13±2.83
3 months	217.20±5.40	0.280±0.026	85.37±2.97	-23.60±3.27	188.10±5.60	0.257±0.047	84.6±0.96	-20.80±1.31
4 months	216.03±5.45	0.343±0.015	84.47±4.43	-17.63±1.02	187.00±2.65	0.253±0.038	86.27±2.43	-24.33±3.96
5 months	217.1±4.70	0.373±0.150	82.19±0.80	-17.73±1.10	207.6±1.90	0.297±0.047	85.63±2.63	-21.93±3.24
6 months	228.8±7.29*	0.385±0.013*	77.66±1.55*	-16.43±0.92*	209.77±6.57	0.290±0.79	84.40±3.21	-18.86±2.00

**Notes:** Data presented as means ± SD (n=3). \*P<0.05 vs initial.

**Abbreviations:** MZL, mizolastine; SLNs, solid lipid nanoparticles; MPS, mean particle size; PDI, polydispersity index; ZP, zeta potential; EE, entrapment efficiency.

These results were found to be in agreement with those obtained by,<sup>55</sup> who reported that, the kinetic modeling of in vitro release profiles of loratadine from SLNs can be described by the anomalous transport or non-Fickian diffusion mechanism.

## Stability Study

The stability of the optimized SLN formulation (F4) was emphasized by checking the physical appearance, PS, PDI, ZP, and EE of MZL throughout the storage period at refrigerated temperature and room temperature for a period of 6 months. During the whole storage period, we could not observe any signs of drug crystallization, phase separation or any modifications in their appearance such as the color and odor in SLNs formulation.

The concern of size stability is more critical for NPs than other drug delivery systems because of their imparted large specific surface area. A comparatively slight increase in the PS was noted ( $202.3 \pm 13.59$  nm) relative to the size prior to freeze drying ( $185.36 \pm 2.56$  nm).

Table 6 illustrated that PS, size distribution, EE, and ZP of F4 were changed from  $202.3 \pm 13.59$  nm,  $0.26 \pm 0.01$ ,

$86.5 \pm 1.47\%$  and  $-22.03 \pm 3.65$  mV, to  $209.77 \pm 6.57$  nm,  $0.290 \pm 0.79$ ,  $84.40 \pm 3.21\%$  and  $-18.86 \pm 2.00$  mV, respectively after 6 months.

It was obvious no extreme alterations in PS, PDI, EE% and ZP ( $P < 0.05$ ) were recorded after the F4 storage at room temperature for a period of 6 months. That showed high stability occasioned by high energy barrier, and more electrostatic repulsion. The ANOVA results clarified the insignificant deviation in those parameters compared with the initial ones all over the storage period at room temperature.

On contrary, at refrigeration condition, the PS of F4 was almost unchanged with maintenance of high ZP values offering high energy barrier and more electrostatic repulsion during the course of this investigation. With the exception a significant increase at ( $P < 0.05$ ) in PS, PDI and a reduction in the EE and ZP values at the 6th month of the storage at refrigerated conditions were recorded.

The polymorphic transition of lipid matrix from a metastable to a stable form leads to the expulsion of drug from the lipid matrix and consequently creates an increase in PS and a reduction in the entrapment capacity.<sup>21,26</sup>

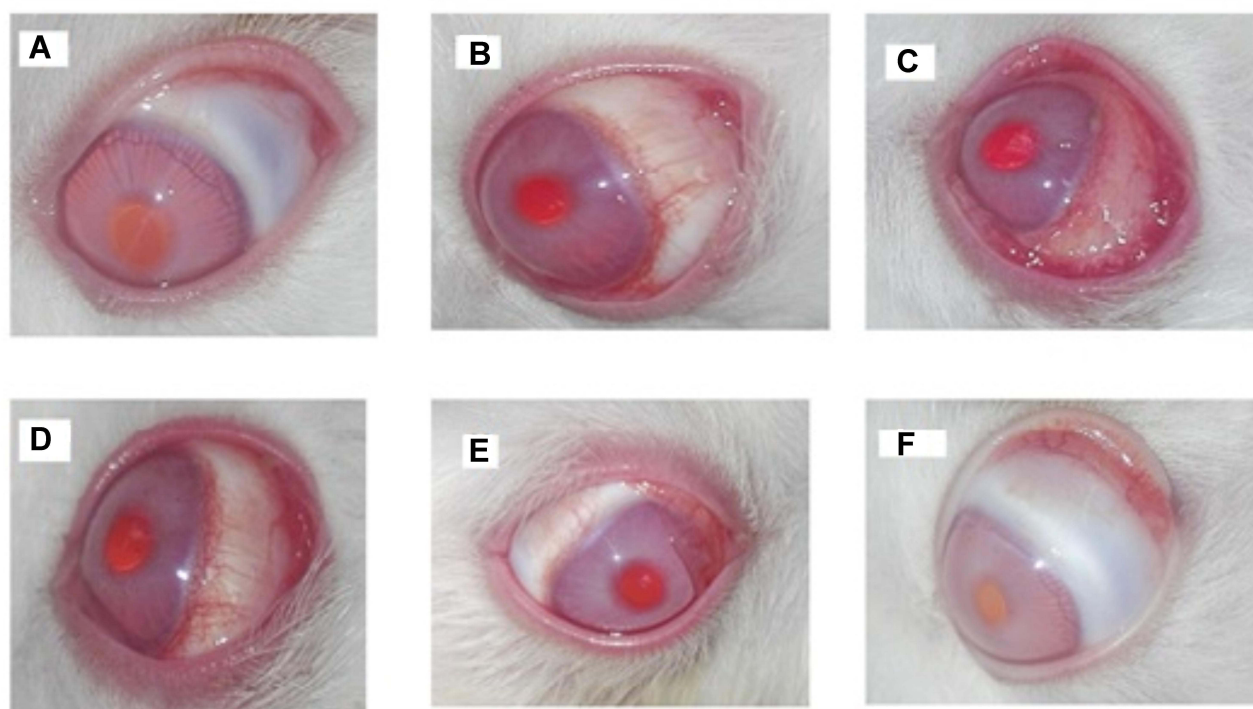


**Figure 8** Gross appearance of normal rabbit-eye normal conjunctiva and cornea with no mucus discharge (A), moderate hyperemia induced after 15 minutes of histamine instillation (B), severe hyperemia induced after 30 minutes of histamine instillation (C), treated with plain hydrogel (D), after 24 hours of treatment with free drug-loaded hydrogel (E), and after 24 hours of treatment with MZL-SLNs hydrogel (F).



The conversion of SLNs into a lyophilized powder can avoid the nanoparticles aggregation and thus, advance their stability. Moreover, the hydrophobicity of lipid long chain fatty acids forms less perfect crystals with many imperfections. As a result, this may interrupt the recrystallization affinity and thus may improve the physical stability of prepared nanoparticles.<sup>56,59</sup>

Therefore, the attained results revealed a strong confirmation of the stability of the freeze dried MZL-loaded SLNs (F4) upon storage for 6 months especially at ambient conditions supplementary its efficiency for a long time.

## Ocular Irritation Evaluation

No signs of irritation, redness, lacrimation or congestion caused by the formulations. Testing the ocular irritation score was done at intervals after administration with zero scoring. Therefore, these results indicated that MZL-SLNs loaded hydrogel formula is a non-irritant to eyes.

## Ophthalmological Examination of Rabbits' Eyes

Figure 8A displayed the gross appearance of normal rabbits' eye indicating normal conjunctiva and cornea with no mucus discharge, while Figure 8B displayed the gross appearance of inflamed rabbits' eye after 15 minutes (moderate redness) and (C) after 30 minutes (severe redness) of histamine solution instillation, respectively.

Figure 8D illustrated the effect of the plain formulation of (sodium alginate/PVP  $\kappa$ 90) hydrogel, showing vascularized diffuse macula and thickened conjunctiva with excessive mucus and no curable symptoms. Whereas, Figure 8E showed the effect of the tested free drug containing hydrogel on the inflamed rabbits' eyes, presenting mild restoration of the normal conjunctival mucosa and less edema.

Regarding the hydrogel formulation containing MZL-SLNs, the complete disappearance of the ocular congestion and repaired conjunctiva were observed after 24 hours (F).

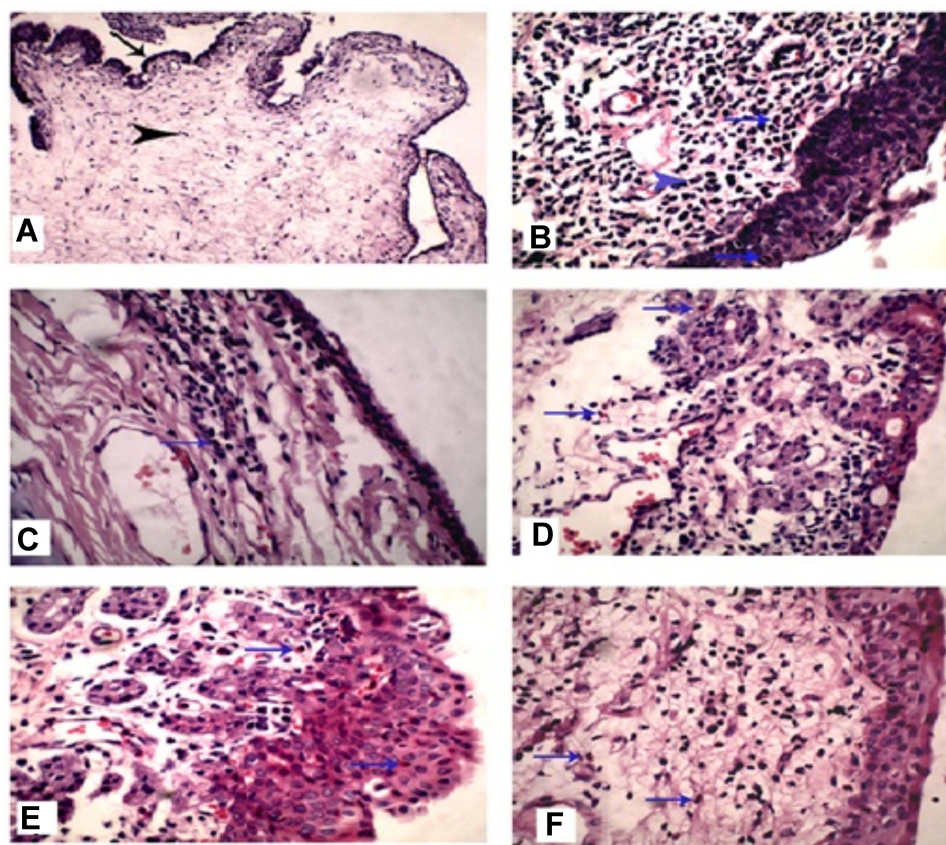


**Figure 9** Microscopy of histopathologic examination of conjunctiva in allergic conjunctivitis-model rabbits after topical application of different gel formulations. Normal control (A), histamine (B), post-treated MZL gel (C), post-treated MZL-SLNs gel (D), pre-treated MZL gel (E) and pre-treated MZL-SLNs gel (F). H&E, 400 $\times$ .

**Notes:** Normal conjunctiva showed stratified epithelia (arrows), and normal submucosa with normal stromal spindle-shaped fibroblasts (arrowheads). The histamine-treated group displayed intense inflammatory exudates with predominance of macrophages, plasma cells (arrowheads) and eosinophilic scattering overlying epithelia (arrows), which indicated hyperplasia and desquamation of the squamous epithelium.

**Table 7** Histological scores for eosinophils, plasma cells, apoptosis, and the thickness of mucosal epithelium in allergic conjunctivitis rabbit model after topical application

	Group I	Group II	Group III	Group IV	Group V	Group VI
Eosinophilic count	0	6.6±0.2	3.25±0.49	2.5±0.35	1.37±0.18	0.5±0.15
Plasma cell count	0	14.2±0.73	7.0±1.4	6.4±0.5	3±0.7	1.2±0.2
Thickness of epithelium (µm)	1.6±0.4	9.2±0.37	5.4±0.24	4.6±0.5	2.0±0.4	1.6±0.24
Apoptosis count	0.6±0.24	7.8±1.02	2.8±0.58	1.6±0.5	0.4±0.24	0.6±0.25
TNF-α count	1.0±0.4	288.8±9.4	173.6±9.6	125.6±6.4	79.4±2.8	28.8±2.8
VEGF count	4.3±0.98	605.8±21.5	447.8±18.75	399.4±5.8	284.4±5.5	188.6±5.5

**Note:** Data presented as means ± SE.

## Histopathological Examination

Allergic conjunctivitis is marked as pathological alterations which characterized by eosinophilic recruitment which being activated by releasing harmful mediators as major basic protein, exotoxins and peroxidase, besides, secretion of pro-inflammatory cytokines such as IL-1α, IL-1β, IL-6 or IL-8 as well as chemokines which have adverse effects on the tissues.<sup>52</sup>

The conjunctiva has high incidence of exposure to multiple allergens and it is a highly sensitive, where, it contains sebaceous glands and apocrine secreting glands that produce the highly essential secretions for eye integrity and vitality. Since allergic inflammatory response in the conjunctiva is detrimental and its severity can be estimated by the number of eosinophilic infiltrates and other detrimental leukocytes in the inflammatory response as plasma cells, macrophages and histiocytes, in addition to pathological alterations in the conjunctival mucosa and associated glandular tissue.

Normal group (Figure 9A) displayed normal mucosa with normal lining epithelium which was approximately five to six layers thick with the goblet cells scattered through the epithelium and normal substantia propria (stroma) consisted of delicate fibrous connective tissue and free from the inflammatory infiltrates. Normal conjunctiva showed stratified epithelium (arrow), and normal submucosa with normal stromal spindle-shaped fibroblast (arrow head). Figure 9B demonstrated the model of allergic conjunctivitis induced by histamine instillation. Histamine treated group displayed intense inflammatory exudate with predominance of macrophages, plasma cells (arrow head) and eosinophilic scattering overlying epithelium (arrow), which announce hyperplasia and desquamation of the squamous epithelium.

Histamine is considered as a potent mediator released from mast cells upon activation by allergen that initiates

allergic conjunctivitis. The histamine exposed conjunctiva displayed intensive eosinophils which became activated and degranulated at the lamina propria invading the conjunctival epithelium. Also, plasma cells and histiocytic infiltrates as immunogenic cells are extensively infiltrating the conjunctival mucosa. The stroma showed hypercellularity of fibroblasts and inflammatory cells. The blood vessels appeared congested and dilated. Moreover, marked hyperplasia and apoptosis were seen in the stratified squamous epithelium in comparison to normal group.

Concerning, group III posttreated with free MZL hydrogel, eosinophils invaded the epithelial layer inducing degenerative changes and hyperplasia. Meanwhile, MZL-SLNs loaded hydrogel post-treated group (IV) had a mild hyperplastic conjunctival epithelium and eosinophils not invaded the epithelium which in contrary to free drug treated group III.

Of all groups, group V pre-treated with free drug loaded hydrogel displayed inflammatory aggregate and moderate eosinophilic recruitment which invades conjunctival mucosa. The stroma exhibited less edema with few inflammatory cells and some dilated blood vessels. While, the pre-treatment of allergic conjunctivitis rabbits' model with MZL-SLNs loaded hydrogel (group VI) restored the normal conjunctival mucosa with nearly normal thickness and normal lamina propria, mild eosinophils and plasma cells infiltrates.

Generally, pre-treatment of allergic conjunctivitis model rabbits with MZL-SLNs loaded hydrogels exhibited improvement of ocular inflammatory manifestations both clinically and by histopathological examination have pronounced inflammatory infiltrates in comparison to post treatment groups. That was detected by significant decrease in the clinical scores. The histological scores for eosinophils, plasma cells, apoptosis and the thickness of mucosal epithelium were shown in Table 7.

The histological scores for eosinophils, plasma cells, apoptosis and the thickness of mucosal epithelium were



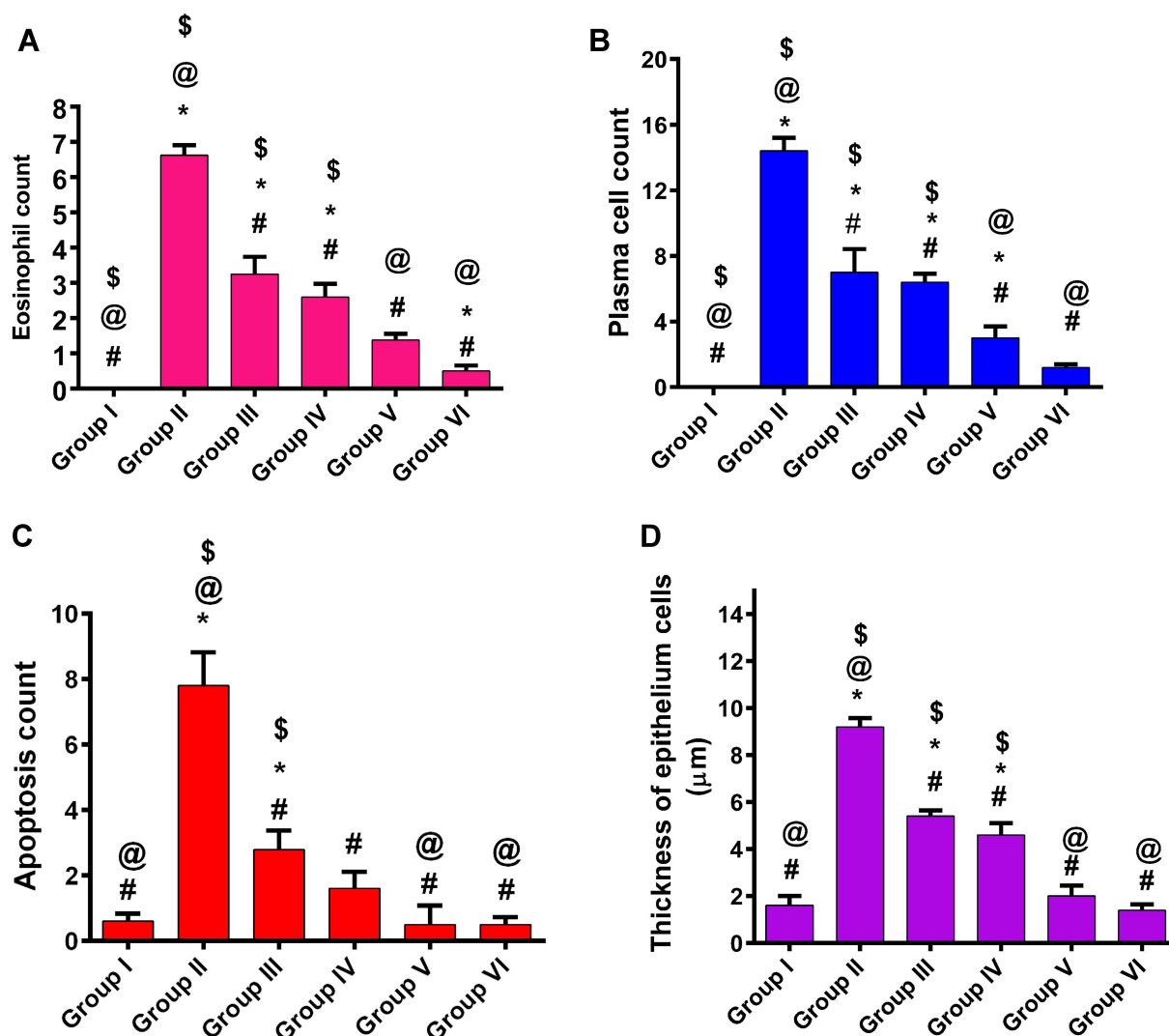


**Figure 10** Effects of mizolastine pre-treatment and post-treatment on histamine-induced increase of eosinophil count (A), plasma cell count (B), thickness of epithelium (C), and apoptosis count (D).

**Notes:**  $P < 0.05$  \*vs normal negative control group, #vs histamine positive-control group, @vs post-treatment with free-drug hydrogel, and \$vs free-drug pre-treatment using Student's t-test (unpaired).

demonstrated statistically differences between different groups at ( $P < 0.05$ ). In general, ocular pretreatment with MZL either free or as SLNs loaded hydrogels lowered the pathologic scores and diminished the allergic symptoms.

The statistical results revealed that there was a significant ( $P < 0.05$ ) elevation in eosinophilic count, plasma cell count, thickness of epithelium and apoptosis count in rabbits' conjunctivae of positive control and post-treated with free drug loaded hydrogel when compared to normal control or pre-treated groups that indicate deleterious alterations in mucosal epithelium and submucosa due to hypersensitivity reaction.

Meanwhile, the ocular posttreatment with MZL-SLNs hydrogels in group IV displayed evidence of pathological

alterations relative to free drug treated group, by time was significantly decreased in eosinophils count, plasma cells recruitment and reduced damage to the epithelium of rabbits' conjunctivae with relatively decreased apoptosis when compared to positive control.

Where groups V and VI pretreated with free MZL loaded hydrogel and MZL-SLNs loaded hydrogel, respectively, were close to the normal group with minimal eosinophilic and plasma cells infiltration (Figure 10 (I & II)), in addition to relatively paucity apoptosis and normal conjunctival thickness (Figure 10 (III&IV)). That insignificant difference between normal control and rabbits' conjunctivae received MZL-SLNs loaded hydrogel regarding severity of all pathological changes may be attributed to the fact that hydrogels containing

MZL-SLNs significantly potentiated the anti-allergic activity of MZL against histamine-induced conjunctivitis in rabbits' model. These results may be due to their nano-size range which results in the mutual enhanced corneal absorption, improving ocular bioavailability on the eye surface and conjunctival sac, prolonging the ocular retention time, and providing a sustained drug release profile. Hence, SLNs can be an effective ocular drug delivery system.<sup>4,47</sup>

Regarding to free MZL either in post or pre-treatment groups, there was a very significant ( $P < 0.05$ ) reduction in these pathological changes only following pretreatment with MZL loaded hydrogel.

## Immunohistochemical Studies

Once eosinophils migrate to the tear film, they attach to specific upregulated adhesion receptors like intercellular adhesion molecule-1 on the activated conjunctival

epithelium through  $\beta 2$ -integrin expressed on the eosinophil surface.<sup>3</sup>

A recent study revealed that conjunctival infection can cause systemic inflammatory responses involving the induction of inflammatory cytokines, including IL-1 $\beta$ , IL-6, IL-8 and TNF- $\alpha$ . It was previously identified that IL-1 $\beta$  is an important inflammatory cytokine, and participates in inflammatory responses to injury and autoimmune diseases.<sup>10</sup>

Also, it has been revealed that epithelial cells, inflammatory cells (eosinophils, monocytes/macrophages) and conjunctival fibroblasts produce VEGF following stimulation.<sup>10,57</sup> Accordingly, it was selected in our study two important biomarkers which are TNF- $\alpha$  and VEGF.

MZL was earlier reported to be effective and well tolerated in the long-term treatment of perennial allergic rhinoconjunctivitis as it has a selective blockade of H<sub>1</sub> receptors.

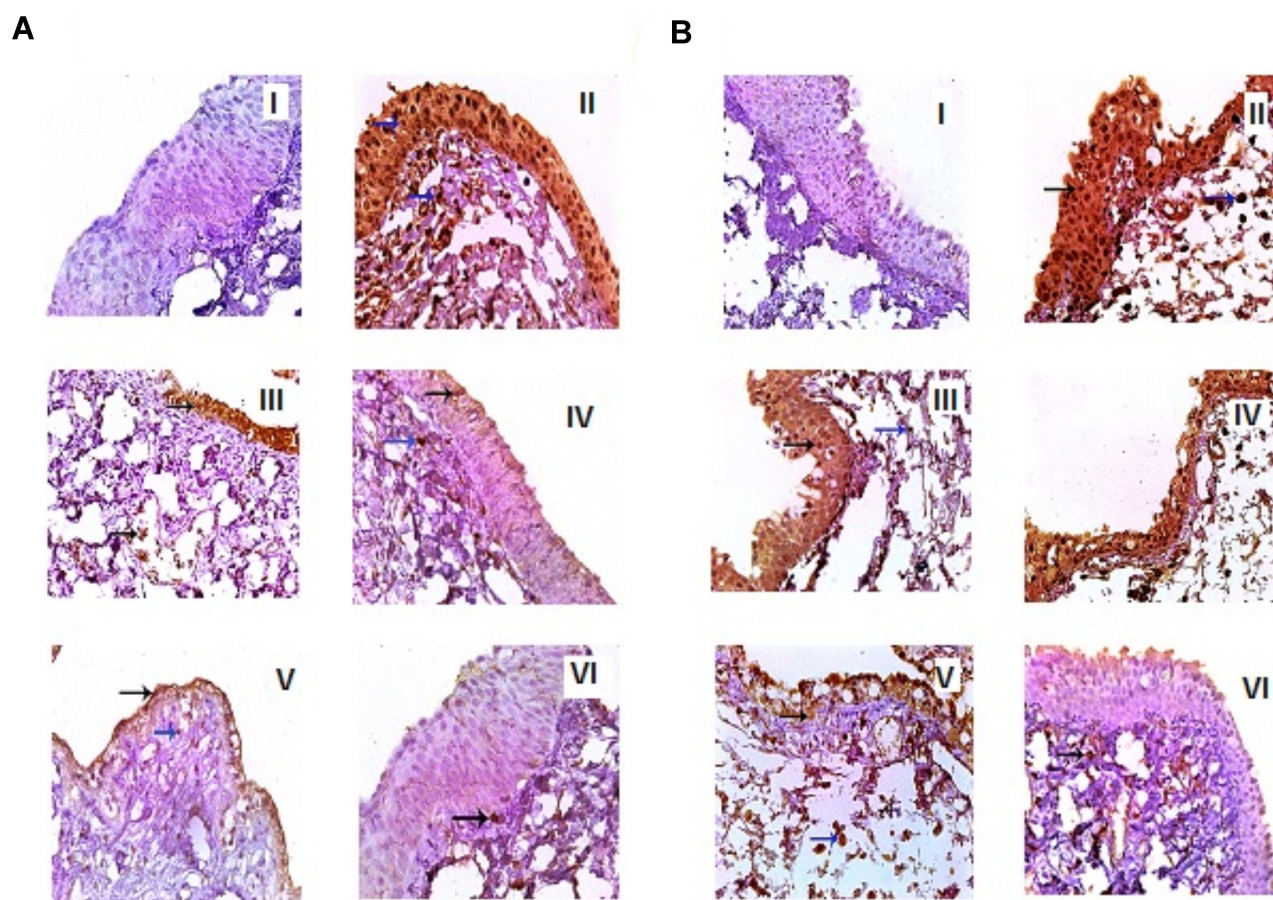


**Figure 11** Microscopy of immunolabeling against TNF- $\alpha$  (A) and VEGF (B) in conjunctiva in allergic conjunctivitis-model rabbits after topical application of different gel formulations: normal control (I), histamine (II), post-treated MZL gel (III), post-treated MZL-SLNs gel (IV), pre-treated MZL gel (V), and pre-treated MZL-SLNs gel (VI).

**Notes:** Immunolabeling against TNF- $\alpha$  and VEGF demonstrated increased or decreased expression at stratified squamous epithelia (black arrows). Expression in fibroblasts and inflammatory cells in the lamina propria shown by blue arrows.

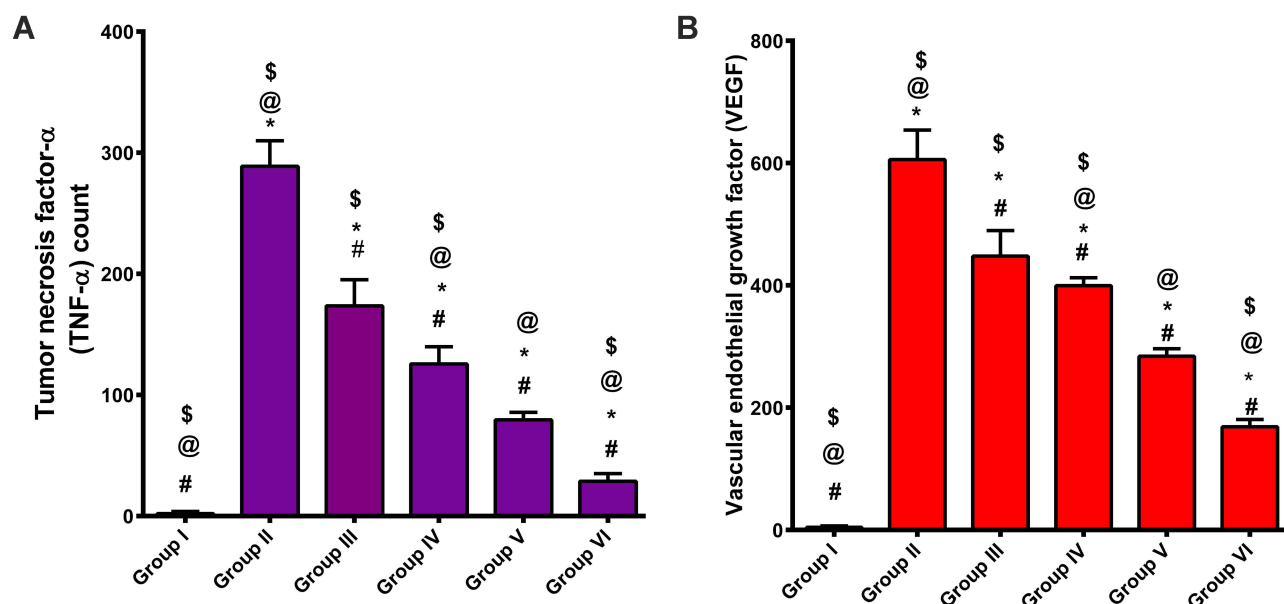


**Figure 12** Effects of mizolastine pre-treatment and post-treatment on histamine-induced increase in expression of TNF- $\alpha$  (A) and VEGF (B) in rabbit conjunctivae in comparison with normal and positive-control groups.

**Notes:**  $P < 0.05$  \*vs normal negative-control group, #vs histamine positive-control group, @vs post-treatment with free-drug hydrogel, \$vs free-drug pre-treatment using Student's *t*-test (unpaired).

In animal models, it was demonstrated to have anti-inflammatory properties with effects persisting for more than 24 hours after a single dose via the inhibition of early and late soluble intercellular adhesion molecule-1 release. However, some anti-allergic effects of MZL observed in animal models, such as inhibition of histamine release from mast cells and inhibition of cell migration.<sup>17,44</sup>

This was reported also in another study that emphasized the fact that, MZL inhibits the release of histamine from rodent mast cells and inhibits the releasing of soluble intercellular adhesion molecule-1 and thus prevents the chemotaxis of the inflammatory cells.<sup>35</sup>

A study investigated by,<sup>11</sup> demonstrated similarly that MZL exerts a significant effect on early phase events, reducing symptoms and pro-inflammatory cytokines.

Figure 11A and B demonstrated the immunolabeling against TNF- $\alpha$  and VEGF, respectively. Immuno-labeling against VEGF and TNF- $\alpha$  demonstrated increased expression at the fibroblasts, inflammatory cells in the lamina propria and stratified squamous epithelium in histamine treated group (II) whereas, negative immunostaining in normal control group (I).

Figure 11A and B (III and IV), indicated that, post-treatment with MZL-SLNs loaded hydrogels suppressed the elevation of TNF- $\alpha$  and VEGF protein expression compared with free MZL hydrogel and control groups.

Group V pre-treated with promising MZL-SLNs loaded hydrogel displayed significant decrease in the expression of both biomarkers in relation to group VI which received the free MZL hydrogel (V& VI).

Statistical analysis using Student's *t*-test (unpaired *t*-test) of positive signal expression of TNF- $\alpha$  and VEGF in both treatment regimens elucidated its significant decrement in rabbits' eyes that received MZL-SLNs hydrogel when compared with positive control or free MZL treated groups (Figure 12A and B).

Ocular posttreatment with free MZL loaded hydrogels insignificantly affect the immunoreactivity. On the other hand, there was a significant ( $P < 0.05$ ) reduction in TNF- $\alpha$  and VEGF expression following MZL-SLNs hydrogels either in pre- or post-treated groups in comparison with the positive control.

In the present study, it was proven that MZL significantly reduces TNF- $\alpha$  and VEGF protein expression levels in rabbits' model of conjunctivitis. The results indicated that the integrated capability of MZL to downregulate these proteins explain the pronounced effect of MZL-SLNs hydrogel.

In agreement with histopathological examination, the superiority of ocular pre- treatment with MZL-SLNs loaded hydrogels over the free drug loaded hydrogel can be suggested by the significantly ( $P < 0.05$ ) lowering of

TNF- $\alpha$  and VEGF protein expression than that produced by either free drug or posttreated with MZL-SLNs loaded hydrogels as well as the insignificantly different from that recorded in normal group. Such superiority may be attributed to the increased intracellular protein expression uptake as well as the improved mucoadhesion and ocular retention of such hydrogels.

A study that has been performed by,<sup>7</sup> demonstrated that SLNs enhance the ocular bioavailability of tobramycin by increasing the residence time on the corneal surface and conjunctiva when compared to an equal dose of tobramycin aqueous solution.

## Conclusion

MZL-SLNs were successfully prepared by hot homogenization followed by ultrasonication technique. The full factorial design paradigm was obeyed to adjust the CQAs. The optimized MZL-SLN (F4) was characterized by the highest EE% (86.5 $\pm$ 1.47%), the smallest MPS (202.3 $\pm$ 13.59 nm), reasonable ZP of -22.03 $\pm$ 3.65 mV. Solid state characterization confirmed that MZL well encapsulated in SLNs as well as the drug was in an amorphous state. TEM and SEM images indicated the formation of spherical particles in nano-size range. In vivo results of this study have confirmed the desirable potential of MZL-SLNs loaded hydrogel to reduce histamine induced symptoms of conjunctivitis in rabbits' eyes model successfully. Moreover, pre-treatment with MZL-SLNs loaded hydrogel imparted a reversal of the abnormal regulation of inflammation as well as marked decreased TNF- $\alpha$  and VEGF expression levels, in rabbits with conjunctivitis in comparison with posttreatment with the same formula. Actually, MZL-SLNs loaded hydrogels deserve deep consideration for their potential future application as a hopeful nanoparticulate system for severe non-infectious allergic conjunctivitis.

## Funding

This work was funded by the authors of this article.

## Disclosure

The authors report no conflicts of interest in this work and declare no competing financial or nonfinancial interests.

## References

- Ackerman S, Smith LM, Gomes PJ. Ocular itch associated with allergic conjunctivitis: latest evidence and clinical management. *Ther Adv Chronic Dis*. 2016;7(1):52–67. doi:10.1177/2040622315612745
- Aman RM, Abu Hashim II, Meshali MM. Novel chitosan-based solid-lipid nanoparticles to enhance the bio-residence of the miraculous phytochemical “apocynin”. *Eur J Pharm Sci*. 2018;124:304–318. doi:10.1016/j.ejps.2018.09.001
- Amin K. The role of mast cells in allergic inflammation. *Respir Med*. 2012;106(1):9–14. doi:10.1016/j.rmed.2011.09.007
- Bachu RD, Chowdhury P, Al-Saedi ZHF, Karla PK, Boddu SHS. Ocular drug delivery barriers—role of nanocarriers in the treatment of anterior segment ocular diseases. *Pharmaceutics*. 2018;10(28):1–31. doi:10.3390/pharmaceutics10010028
- Bansal H, Khatry S, Arora S. Formulation and evaluation of programmed release ocular inserts of mizolastine. *Int J Pharm Sci Res*. 2013;4(1):497–501.
- Butani D, Yewale C, Misra A. Topical amphotericin B solid lipid nanoparticles: design and development. *Colloids Surf B Biointerfaces*. 2016;139:17–24. doi:10.1016/j.colsurfb.2015.07.032
- Cavalli R, Gasco MR, Chetoni P, Burgalassi S, Saettone MF. Solid Lipid Nanoparticles (SLN) as ocular delivery system for tobramycin. *Int J Pharm*. 2002;238(1–2):241–245. doi:10.1016/S0378-5173(02)00080-7
- Cavendish M, Nalane L, Barbosa T, et al. Study of pre-formulation and development of solid lipid nanoparticles containing perillyl alcohol. *J Therm Anal Calorim*. 2019;141(2):767–774. doi:10.1007/s10973-019-09080-0
- Chen R, Wang S, Zhang J, Chen M, Wang Y. Aloe-Emodin loaded solid lipid nanoparticles: formulation design and in vitro anti-cancer study. *Drug Deliv*. 2015;22(5):666–674. doi:10.3109/10717544.2014.882446
- Chen Y, Hong X. Effects of carvedilol reduce conjunctivitis through changes in inflammation, Ngf and Vegf levels in a rat model. *Exp Ther Med*. 2016;11(5):1987–1992. doi:10.3892/etm.2016.3140
- Ciprandi G, Cirillo I, Vizzaccaro A. Mizolastine and fexofenadine modulate cytokine pattern after nasal allergen challenge. *Eur Ann Allergy Clin Immunol*. 2004;36(4):146–150.
- Córdova C, Gutiérrez B, Martínez-García C, et al. Oleanolic acid controls allergic and inflammatory responses in experimental allergic conjunctivitis. *PLoS One*. 2014;9(4):e91282. doi:10.1371/journal.pone.0091282
- Danaei M, Dehghankhold M, Ataei S, et al. Impact of particle size and polydispersity index on the clinical applications of lipidic nanocarrier systems. *Pharmaceutics*. 2018;10(2):57. doi:10.3390/pharmaceutics10020057
- Dandagi PM, Dessai GA, Gadad AP, Desai VB. Formulation and evaluation of nanostructured lipid carrier (NLC) of lornoxicam. *Int J Pharm Pharm Sci*. 2014;6(2):73–77.
- Date AA, Nagarsenker MS. Single-Step and low-energy method to prepare solid lipid nanoparticles and nanostructured lipid carriers using biocompatible solvents. *Eur J Pharm Res*. 2019;1(1):12–19. doi:10.34154/2019-EJPR.01(01).pp-12-19/eurass
- De Oliveira GGG, Feitosa A, Loureiro K, Fernandes AR, Souto EB, Severino P. Compatibility study of paracetamol, chlorpheniramine maleate and phenylephrine hydrochloride in physical mixtures. *Saudi Pharm J*. 2017;25(1):99–103. doi:10.1016/j.jsps.2016.05.001
- Del Cuvillo A, Sastre J, Montoro J, et al. Allergic conjunctivitis and H. *J Investig Allergol Clin Immunol*. 2009;19(1):11–18.
- Deza G, Giménez-Arnau AM. Management and treatment of contact urticaria syndrome. In: *Contact Urticaria Syndrome: Diagnosis and Management*. Giménez-Arnau AM, Maibach HI, editors. Cham: Springer International Publishing; 2018:161–170.
- Dong S, Wu X, Xu Y, Yang G, Yan M. (Immunohistochemical study of Stat3, Hif-1 $\alpha$  and Vegf in pterygium and normal conjunctiva: experimental research and literature review). *Mol Vis*. 2020;26:510–516.
- Draize JH, Woodard G, Calvery HO. Methods for the study of irritation and toxicity of substances applied topically to the skin and mucous membranes. *J Pharmacol Exp Ther*. 1944;82:377–390.



21. Dudhipala N, Veerabrahma K. Candesartan cilexetil loaded solid lipid nanoparticles for oral delivery: characterization, pharmacokinetic and pharmacodynamic evaluation. *Drug Deliv.* 2016;23:395–404. doi:10.3109/10717544.2014.914986
22. Emami J, Yousefian H, Sadeghi H. Targeted nanostructured lipid carrier for brain delivery of artemisinin: design, preparation, characterization, optimization and cell toxicity. *J Pharm Pharm Sci.* 2018;21:225s–241s. doi:10.18433/jpps30117
23. Garud A, Singh D, Garud N. Solid Lipid Nanoparticles (SLN): method, characterization and applications. *Int Curr Pharm.* 2012;1(11):384–393. doi:10.3329/icpj.v1i11.12065
24. Gazi AS, Sailaja AK. Preparation and evaluation of paracetamol solid lipid nanoparticle by hot homogenization method. *J Nanomed Res.* 2018;7(2):152–154. doi:10.15406/jnmr.2018.07.00184
25. Ghanbarzadeh S, Hariri R, Kouhsoltani M, Shokri J, Javadzadeh Y, Hamishehkar H. Enhanced stability and dermal delivery of hydroquinone using solid lipid nanoparticles. *Colloids Surf B Biointerfaces.* 2015;136:1004–1010. doi:10.1016/j.colsurfb.2015.10.041
26. Gordillo-Galeano A, Mora-Huertas CE. Solid lipid nanoparticles and nanostructured lipid carriers: a review emphasizing on particle structure and drug release. *Eur J Pharm Biopharm.* 2018;133:285–308.
27. Gupta S, Kesarla R, Chotai N, Misra A, Omri A. Systematic approach for the formulation and optimization of solid lipid nanoparticles of efavirenz by high pressure homogenization using design of experiments for brain targeting and enhanced bioavailability. *Biomed Res Int.* 2017;18. doi:10.1155/2017/5984014
28. Kang JH, Chon J, Kim YI, et al. Preparation and evaluation of tacrolimus-loaded thermosensitive solid lipid nanoparticles for improved dermal distribution. *Int J Nanomedicine.* 2019;14:5381–5396. doi:10.2147/IJN.S215153
29. Karn-Orachai K, Smith SM, Saesoo S, et al. Surfactant effect on the physicochemical characteristics of I-oryanol-containing solid lipid nanoparticles. *Colloids Surf a Physicochem Eng.* 2016;488:118–128. doi:10.1016/j.colsurfa.2015.10.011
30. Khames A, Khaleel MA, El-Badawy MF, El-Nezhawy AOH. Natamycin solid lipid nanoparticles–sustained ocular delivery system of higher corneal penetration against deep fungal keratitis: preparation and optimization. *Int J Nanomedicine.* 2019;14:2515–2531. doi:10.2147/IJN.S190502
31. Kovacevic A, Savic S, Vuleta G, Müller RH, Keck CM. Polyhydroxy surfactants for the formulation of lipid nanoparticles (SLN and NLC): effects on size, physical stability and particle matrix structure. *Int J Pharm.* 2011;406:163–172. doi:10.1016/j.ijpharm.2010.12.036
32. Kumar R, Singh A, Garg N, Siril PF. Solid lipid nanoparticles for the controlled delivery of poorly water soluble non-steroidal anti-inflammatory drugs. *Ultrason Sonochem.* 2018;40:686–696. doi:10.1016/j.ultrasonch.2017.08.018
33. Kumar R, Sinha VR. Lipid nanocarrier: an efficient approach towards ocular delivery of hydrophilic drug (valacyclovir). *AAPS PharmSciTech.* 2017;18:884–894. doi:10.1208/s12249-016-0575-2
34. Mandola A, Nozawa A, Eiwegger T. Histamine, histamine receptors, and anti-histamines in the context of allergic responses. *Lympho Sign J.* 2019;6:35–51. doi:10.14785/lymphosign-2018-0016
35. Lebrun-Vignes B, Diquet B, Chosidow O. Clinical pharmacokinetics of mizolastine. *Clin Pharmacokinet.* 2001;40(7):501–507. doi:10.2165/00003088-200140070-00002
36. Moghddam SMM, Ahad A, Aqil M, Imam SS, Sultana Y. Optimization of nanostructured lipid carriers for topical delivery of nimesulide using box–behnen design approach. *Artif Cells Nanomed Biotechnol.* 2017;45(3):617–624. doi:10.3109/21691401.2016.1167699
37. Müller RH, Maeder K, Gohla S. Solid Lipid Nanoparticles (SLN) for controlled drug delivery—a review of the state of the art. *Eur J Pharm Biopharm.* 2000;50:161–177. doi:10.1016/S0939-6411(00)00087-4
38. Müller RH, Radtke M, Wissing SA. ‘Solid Lipid Nanoparticles (SLN) and Nanostructured Lipid Carriers (NLC) in cosmetic and dermatological preparations. *Adv Drug Deliv Rev.* 2002;54:S131–S55. doi:10.1016/S0169-409X(02)00118-7
39. Natarajan J, Baskaran M, Humtsoe LC, Vadivelan R, Justin A. Enhanced brain targeting efficacy of olanzapine through solid lipid nanoparticles. *Artif Cells Nanomed Biotechnol.* 2017;45:364–371. doi:10.3109/21691401.2016.1160402
40. Niu Z, Conejos-Sánchez I, Griffin BT, O’Driscoll CM, Alonso MJ. Lipid-based nanocarriers for oral peptide delivery. *Adv Drug Deliv Rev.* 2016;106:337–354. doi:10.1016/j.addr.2016.04.001
41. Petkar KC, Chavhan S, Kunda N, et al. Development of novel octanoyl chitosan nanoparticles for improved rifampicin pulmonary delivery: optimization by factorial design. *AAPS PharmSciTech.* 2018;19:1758–1772. doi:10.1208/s12249-018-0972-9
42. Ritger PL, Peppas NA. A simple equation for description of solute release I. Fickian and Non-Fickian release from non-swelling devices in the form of slabs, spheres, cylinders or discs. *J Control Release.* 1987;5:23–36. doi:10.1016/0168-3659(87)90034-4
43. Sánchez-López E, Espina M, Doktorovova S, Souto EB, García ML. Lipid nanoparticles (SLN, NLC): overcoming the anatomical and physiological barriers of the eye–Part I: ocular drug-loaded lipid nanoparticles. *Eur J Pharm Biopharm.* 2017;110:58–69. doi:10.1016/j.ejpb.2016.10.013
44. Scadding GK, Tasman AJ, Murrieta-Aguttes M, Bachert C; Riperex Study Group. Mizolastine is effective and well tolerated in long-term treatment of perennial allergic rhinoconjunctivitis. *J Int Med Res.* 1999;27:273–285. doi:10.1177/030006059902700603
45. Sebbag L, Allbaugh RA, Weaver A, Seo YJ, Mochel JP. Histamine-induced conjunctivitis and breakdown of blood–tear barrier in dogs: a model for ocular pharmacology and therapeutics. *Front Pharmacol.* 2019;10(752):1–11. doi:10.3389/fphar.2019.00752
46. Seyed YA, Shahidi F, Mohebbi M, Varidi M, Golmohammadzadeh S. The effect of different lipids on physicochemical characteristics and stability of phycocyanin-loaded solid lipid nanoparticles. *Iran J Food Sci Technol.* 2017;14(67):83–93.
47. Seyfoddin A, Shaw J, Al-Kassas R. Solid lipid nanoparticles for ocular drug delivery. *Drug Deliv.* 2010;17:467–489. doi:10.3109/10717544.2010.483257
48. Shah R, Eldridge D, Palombo E, Harding I. Optimisation and stability assessment of solid lipid nanoparticles using particle size and zeta potential. *J Phys Sci.* 2014;25(1):59–75.
49. Shazly GA. Ciprofloxacin controlled-solid lipid nanoparticles: characterization, in vitro release, and antibacterial activity assessment. *Biomed Res Int.* 2017;9. doi:10.1155/2017/2120734
50. Shokry M, Hathout RM, Mansour S. Exploring gelatin nanoparticles as novel nanocarriers for timolol maleate: augmented in-vivo efficacy and safe histological profile. *Int J Pharm.* 2018;545:229–239. doi:10.1016/j.ijpharm.2018.04.059
51. Singh M, Guzman-Arangué A, Hussain A, Srinivas CS, Kaur IP. Solid lipid nanoparticles for ocular delivery of isoniazid: evaluation, proof of concept and in vivo safety & kinetics. *Nanomedicine.* 2019;14:465–491. doi:10.2217/nnm-2018-0278
52. Stojković N, Cekić S, Ristov M, et al. Histamine and antihistamines/histamin I antihistamin. *Acta Facultatis Medicae Naissensis.* 2015;32:7–22. doi:10.1515/afmna-2015-0001
53. Sut TN, Jackman JA, Yoon BK. Influence of NaCl concentration on bicelle-mediated SLB formation. *Langmuir.* 2019;35(32):10658–10666. doi:10.1021/acs.langmuir.9b01644
54. Sznitowska M, Wolska E, Baranska H, Cal K, Pietkiewicz J. The effect of a lipid composition and a surfactant on the characteristics of the solid lipid microspheres and nanospheres (SLM and SLN). *Eur J Pharm Biopharm.* 2017;110:24–30. doi:10.1016/j.ejpb.2016.10.023



55. Üner M, Karaman EF, Aydoğmuş Z. Solid lipid nanoparticles and nanostructured lipid carriers of loratadine for topical application: physicochemical stability and drug penetration through rat skin. *Trop J Pharm Res.* 2014;13:653–660. doi:10.4314/tjpr.v13i5.1
56. Vivek K, Reddy H, Murthy RS. Investigations of the effect of the lipid matrix on drug entrapment, in vitro release, and physical stability of olanzapine-loaded solid lipid nanoparticles. *AAPS PharmSciTech.* 2007;8:16–24. doi:10.1208/pt0804083
57. Wang F, Xu P, Xie KC, Chen XF, Li CY, Huang Q. Effects of tumor microenvironmental factors on VEGF expression. *Biomed Rep.* 2013;1:539–544. doi:10.3892/br.2013.115
58. Wei CC, Kung YJ, Chen CS, et al. Allergic conjunctivitis-induced retinal inflammation promotes myopia progression. *EBioMedicine.* 2018;28:274–286. doi:10.1016/j.ebiom.2018.01.024
59. Westesen K, Bunjes H, Koch MHJ. Physicochemical characterization of lipid nanoparticles and evaluation of their drug loading capacity and sustained release potential. *J Control Release.* 1997;48:223–236. doi:10.1016/S0168-3659(97)00046-1
60. Wissing SA, Kayser O, Müller RH. Solid lipid nanoparticles for parenteral drug delivery. *Adv Drug Deliv Rev.* 2004;56:1257–1272. doi:10.1016/j.addr.2003.12.002
61. Xiong X, Song L, Chen F, Ma X. Effects of combination of mizolastine and proteoglycan on chronic urticaria: a randomized controlled trial. *Arch Dermatol Res.* 2019;311:801–805. doi:10.1007/s00403-019-01967-0
62. Yang M, Chen X, Wang Y, et al. Comparative evaluation of thermal decomposition behavior and thermal stability of powdered ammonium nitrate under different atmosphere conditions. *J Hazard Mater.* 2017;337:10–19. doi:10.1016/j.jhazmat.2017.04.063
63. Yang X, Trinh HM, Agrahari V, Sheng Y, Pal D, Mitra AK. Nanoparticle-based topical ophthalmic gel formulation for sustained release of hydrocortisone butyrate. *AAPS PharmSciTech.* 2016;17:294–306. doi:10.1208/s12249-015-0354-5

## International Journal of Nanomedicine

Dovepress

### Publish your work in this journal

The International Journal of Nanomedicine is an international, peer-reviewed journal focusing on the application of nanotechnology in diagnostics, therapeutics, and drug delivery systems throughout the biomedical field. This journal is indexed on PubMed Central, MedLine, CAS, SciSearch®, Current Contents®/Clinical Medicine,

Journal Citation Reports/Science Edition, EMBase, Scopus and the Elsevier Bibliographic databases. The manuscript management system is completely online and includes a very quick and fair peer-review system, which is all easy to use. Visit <http://www.dovepress.com/testimonials.php> to read real quotes from published authors.

Submit your manuscript here: <https://www.dovepress.com/international-journal-of-nanomedicine-journal>